Draft version June 11, 2014
Preprint typeset using LaTeX style emulateapj v. 5/2/11

arXiv:1406.2327v1 [astro-ph.GA] 9 Jun 2014

LATE-STAGE GALAXY MERGERS IN COSMOS TO $Z \sim 1$

C. N. Lackner[1], J. D. Silverman[1], M. Salvato[2], P. Kampczyk[3], J. S. Kartaltepe[4], D. Sanders[5], P. Capak[6], F. Civano[7,8], O. Ilbert[9], K. Jahnke[10], A. M. Koekemoer[11], N. Lee[5], O. Le Fèvre[9], C. T. Liu[12], N. Scoville[6], K. Sheth[13], and S. Toft[14]

Draft version June 11, 2014

ABSTRACT

The role of major mergers in galaxy and black hole formation is not well constrained. To help address this, we develop an automated method to identify late-stage galaxy mergers before coalescence of the galactic cores. The resulting sample of mergers is distinct from those obtained using pair-finding and morphological indicators. Our method relies on median-filtering of high-resolution images in order to distinguish two concentrated galaxy nuclei at small separations. This method does not rely on low surface brightness features to identify mergers, and is therefore reliable to high redshift. Using mock images, we derive statistical contamination and incompleteness corrections for the fraction of late-stage mergers. The mock images show that our method returns an uncontaminated ($< 10\%$) sample of mergers with projected separations between 2.2 and 8 kpc out to $z \sim 1$. We apply our new method to a magnitude-limited ($m_{FW814} < 23$) sample of 44164 galaxies from the COSMOS *HST*/ACS catalog. Using a mass-complete sample with $\log M_*/M_\odot > 10.6$ and $0.25 < z \leq 1.00$, we find $\sim 5\%$ of systems are late-stage mergers. Correcting for incompleteness and contamination, the fractional merger rate increases strongly with redshift as $\Re_{\rm merge} \propto (1+z)^{3.8\pm0.9}$, in agreement with earlier studies and with dark matter halo merger rates. Separating the sample into star-forming and quiescent galaxies shows that the merger rate for star-forming galaxies increases strongly redshift, $(1+z)^{4.5\pm1.3}$, while the merger rate for quiescent galaxies is consistent with no evolution, $(1+z)^{1.1\pm1.2}$. The merger rate also becomes steeper with decreasing stellar mass. Limiting our sample to galaxies with spectroscopic redshifts from zCOSMOS, we find that the star formation rates and X-ray selected AGN activity in likely late-stage mergers are enhanced by factors of ~ 2 relative to a control sample. Combining our sample with more widely separated pairs, we find that $8 \pm 5\%$ of star formation and $20 \pm 8\%$ of AGN activity is triggered by close encounters (< 143 kpc) or mergers, once more suggesting that major mergers are not the only channels for star formation and black hole growth.

Subject headings: galaxies: active – galaxies: formation – galaxies: interactions – techniques: image processing

1. INTRODUCTION

In a hierarchical universe, galaxies grow by accretion of gas and mergers. Dark matter simulations suggest that the halo merger rate (in units per Gyr) increases with redshift as $(1+z)^{2-3}$ (Lacey & Cole 1993; Fakhouri et al. 2010). However, identifying merging galaxies and transforming those observations into a galaxy merger rate is not easy, as is evidenced by the large differences between different methods (see Patton & Atfield 2008; De Propris et al. 2007; Bell et al. 2006; Jogee et al. 2009; Lotz et al. 2011, and references therein). Many of the differences in merger rates are due to differences in sample selection and merger identification (see Lotz et al. 2011). Nonetheless, a precise determination of the merger rate of galaxies is essential to the study of galaxy growth. In particular, the galaxy merger rate is needed to compare the growth of galaxies to the growth of dark matter halos. Galaxy mergers may also play an important role in shaping galaxy morphology (Toomre & Toomre 1972; Sanders et al. 1988; Barnes & Hernquist 1992; Hopkins et al. 2009), instigating star formation (Mihos et al. 1992; Sanders & Mirabel 1996; Barton et al. 2000; Lambas et al. 2003; Ellison et al. 2008; Patton et al. 2013), and inducing super-massive black hole growth (e.g., Hernquist 1989; Moore et al. 1996; Hopkins et al. 2008; Di Matteo et al. 2008).

There are two general classes of methods for finding galaxy mergers. The first class of methods selects close pairs of galaxies, before the galaxies have merged (e.g., López-Sanjuan et al. 2013, 2011, 2012; Bundy et al.

claire.lackner@ipmu.jp
[1] Kavli IPMU (WPI), The University of Tokyo, Kashiwa, Chiba 277-8583, Japan
[2] Max-Planck-Institut für extraterrestrische Physik, D-84571 Garching, Germany
[3] Institute of Astronomy, Department of Physics, ETH Zürich, CH-8093 Zürich, Switzerland
[4] National Optical Astronomy Observatory, Tucson, AZ 85719, USA
[5] Institute for Astronomy, University of Hawaii, Honolulu, HI 96822
[6] California Institute of Technology, Pasadena, CA 91125
[7] Harvard-Smithsonian Center for Astrophysics, Cambridge, MA 02138
[8] Department of Physics and Astronomy, Dartmouth College, Hanover, NH 03755
[9] Aix Marseille Université, CNRS, LAM (Laboratoire dAstrophysique de Marseille), 13388, Marseille, France
[10] Max-Planck-Institut für Astronomie, D-69117 Heidelberg, Germany
[11] Space Telescope Science Institute, Baltimore, MD 21218
[12] Astrophysical Observatory, CUNY, College of Staten Island, NY 10314 USA
[13] National Radio Astronomy Observatory/NAASC, Charlottesville, VA 22903
[14] Dark Cosmology Centre, Niels Bohr Institute, University of Copenhagen, Copenhagen, DK-2100 Denmark

2009; Lin et al. 2004, 2010; Patton & Atfield 2008; Kartaltepe et al. 2007; de Ravel et al. 2009; Bell et al. 2006; Masjedi et al. 2008; Ellison et al. 2008; Williams et al. 2011; Robaina et al. 2010; Newman et al. 2012; Ellison et al. 2013; Tasca et al. 2014). These methods typically select galaxies with projected separations less than $100\,h_{100}^{-1}$ kpc. The line-of-sight separation depends on the method used. Galaxy mergers selected using photometric redshifts include pairs that are widely separated along the line-of-sight and will never merge (e.g., Kartaltepe et al. 2007; Bundy et al. 2009; López-Sanjuan et al. 2011, 2012). Although these methods cannot identify individual chance superpositions, superpositions can be easily accounted for statistically in merger-rate calculations (e.g. Bundy et al. 2009; López-Sanjuan et al. 2011, 2012). In order to better distinguish chance superpositions from actual mergers, several studies utilize spectroscopic redshifts and identify kinematic pairs of galaxies (e.g., Lin et al. 2004; Patton & Atfield 2008; de Ravel et al. 2009; de Ravel et al. 2011; Kampczyk et al. 2013; Ellison et al. 2013; López-Sanjuan et al. 2013). For spectroscopic samples, understanding the completeness of the spectroscopy as a function of galaxy separation is essential (Kampczyk et al. 2013; Patton & Atfield 2008; Lin et al. 2004). Although kinematic pairs eliminate many chance superpositions from a sample of galaxy mergers, spectroscopic samples contain far fewer galaxies than photometric samples and often miss close pairs due to fiber collisions, leading to poorer statistics when measuring galaxy merger rates.

The second class of methods for finding galaxy mergers looks for morphological signatures during or after a merger (e.g., double nuclei, tidal tails, outer shells). Morphological searches either involve visual inspection (e.g., Kartaltepe et al. 2014, 2010; Kampczyk et al. 2007; Jogee et al. 2009; Bridge et al. 2010; Cisternas et al. 2011), or quantitative, non-parametric measures of galaxy morphology (e.g., Lotz et al. 2008a; Conselice et al. 2009; Scarlata et al. 2007; Shi et al. 2009; De Propris et al. 2007; López-Sanjuan et al. 2009). Visual inspection involves searches for merger signatures, some obvious, such as double nuclei, and some subtle, such as sharp breaks in the radial light profile. Measurements, such as the the central concentration, asymmetry, and clumpiness (CAS) (Abraham et al. 1994; Conselice 2003), the second moment of the light profile (M_{20}) (Lotz et al. 2004), and the Gini coefficient of the 2-dimensional flux distribution (Abraham et al. 2003; Lotz et al. 2004), seek to quantify the morphological signatures of bulges, disks, and galaxy mergers. By comparing visual classification with these quantitative measures, Lotz et al. (2004) demonstrate that major mergers occupy a distinct part of the Gini-M_{20}-concentration-asymmetry space. However, neither visual classification nor non-parametric morphology methods directly measure the merger mass ratio and do not distinguish between major and minor mergers. In fact, morphology-based methods are sensitive to very minor mergers and even close passages which cause morphological disturbances without leading to a merger (see Lotz et al. 2011).

Both pair-finding methods and morphology-based methods are used to measure the galaxy merger fraction and its evolution. The methods are applied to many data sets with various selection functions. The resulting fractions of merging galaxies at $z \sim 0.5$ vary from $1 - 20\%$ and the evolution of the merger rate is either very steep, $(1+z)^4$, or non-existent, $(1+z)^0$. Several works address these differences (e.g., Patton & Atfield 2008; Jogee et al. 2009; Lotz et al. 2011). Some of the differences may be due to the parent sample selection with redshift; samples selected at fixed number density show a different merger rate evolution than those selected at fixed stellar mass (Lotz et al. 2011). Additionally, the length of time each method is sensitive to a galaxy merger is highly uncertain and varies greatly as a function of merger-finding method and as a function of redshift and merger mass ratio. Both photometric pair-finding methods and morphological methods mis-identify galaxy mergers and often select chance superpositions of galaxies that are widely separated along the line of sight. Spectroscopic pair studies greatly limit the number of line-of-sight pairs, however. Morphology-based methods often select galaxies in which close passages or very minor mergers caused dramatic morphological disturbances. While most studies correct for these mis-identifications, the correction factor is difficult to accurately calculate. The typical assumed fraction of mis-identified mergers ranges from 0 to 60% (see Lotz et al. 2011, and references therein).

In this work, we present a new quantitative method for identifying merging galaxies. Our method is in essence a high-pass filter which makes multiple peaks in galaxy surface brightness profiles easily distinguishable. The method is designed to select a sample of late-stage mergers in which two galaxy nuclei are still intact and only separated by a few kpc. In particular, we select galaxies whose nuclei are separated by $2.2-8$ kpc, and expected to merge within a few hundred Myr (see Lotz et al. 2011). These galaxies lie at the interface between early-stage galaxy mergers selected in close pair studies and post-merger galaxies selected based on disturbed morphologies. Indeed, we show below our sample of late-stage mergers has little overlap with kinematically selected, more widely separated pairs. At separations of a few kpc, it is less likely that the galaxy pair is a chance superposition than at larger separations (e.g. Kartaltepe et al. 2007), reducing contamination from spurious pairs. By eliminating pairs that are likely to be spurious mergers, our estimates of the merger rate are robust and competitive with other merger-finding methods, including searches for spectroscopic pairs. While many galaxies in our sample could be selected by visual inspection, in practice there is little overlap between mergers identified by other quantitative morphology methods (e.g., Gini-M_{20}, asymmetry) and our sample of late-stage mergers. This is likely due to the fact galaxies with two very close, equally-bright central peaks will not have abnormally large asymmetry or second moment measurements.

In addition to the number of merging galaxies, the properties of merging galaxies are also of much interest. Numerical simulations of merging galaxies demonstrate that major mergers can drive gas toward the center of galaxies leading to enhanced star formation, efficient bulge creation, and AGN activity as some of the gas is deposited on the central black hole (e.g.,

Hernquist 1989; Mihos et al. 1992; Barnes & Hernquist 1992; Hopkins et al. 2008, 2006). Several observational studies have shown that merging galaxies typically have enhanced star formation (e.g., Kartaltepe et al. 2012; Robaina et al. 2009; Xu et al. 2012; Kampczyk et al. 2013; Hung et al. 2013). Indeed, almost all intensely star-forming systems, such as luminous infrared galaxies (LIRGS), in the local universe have morphologies consistent with major mergers (Sanders & Mirabel 1996; Wu et al. 1998; Cui et al. 2001; Kartaltepe et al. 2010). Similarly, several studies between $z \sim 0$ and $z \sim 1.2$ show an enhancement in the fraction of close galaxy pairs with AGN activity compared to isolated galaxies (e.g., Kennicutt & Keel 1984; Keel et al. 1985; Alonso et al. 2007; Silverman et al. 2011; Koss et al. 2011; Ellison et al. 2013; Satyapal et al. 2014, but see Darg et al. 2010a; Li et al. 2008; Ellison et al. 2008). Nonetheless, the majority of low-luminosity AGN activity is not associated with merging galaxies (e.g., Cisternas et al. 2011; Kocevski et al. 2012; Kauffmann et al. 2004; Silverman et al. 2011). Using COSMOS *HST* images, Cisternas et al. (2011) find that X-ray selected AGN are no more likely to be ongoing or recent major mergers than a control sample of inactive galaxies. Silverman et al. (2011) examine close kinematic pairs with separations less than 75kpc and find that 18% of X-ray selected AGN activity since $z \sim 1$ is triggered by interactions of close pairs. Including late-stage mergers will increase the completeness of pairs at separations less than 10 kpc and boost the fraction of AGN associated with merging. Late-stage mergers may help explain a significant fraction of the AGN activity not currently associated with galaxy pairs. Furthermore, understanding galaxy properties as a function of time to coalescence can help test numerical models of merging galaxies and black hole growth (e.g., Hopkins et al. 2006; Di Matteo et al. 2007; Mihos et al. 1992).

In this study, we apply our method, which selects galaxies likely undergoing late-stage mergers, to a flux-limited sample of 44164 galaxies from the COSMOS survey. Because we are looking at high redshift and therefore require high spatial resolution to separate galaxy pairs, we apply our pair-finding method to *Hubble Space Telescope* (*HST*) images taken as a part of the COSMOS survey (Scoville et al. 2007; Koekemoer et al. 2007). The galaxies are selected from the ACS galaxy catalog (Leauthaud et al. 2007). Photometric redshifts, stellar masses, and absolute magnitudes are taken from the most recent near infrared-selected COSMOS catalog (Ilbert et al. 2013; McCracken et al. 2012). The data and merger-finding method are described in detail in §2 and §3. The sample of 2047 late-stage mergers is presented in Table 2. Thirty-two of these late-stage mergers are also detected in X-ray by either *Chandra* or *XMM*.

We test the robustness of our method using simulated images of mergers in §3.1. After demonstrating that our selection of late mergers is almost independent of redshift, we calculate the galaxy merger rate as a function of redshift between $0.25 \leq z < 1.0$ (§4). Finally, we analyze the star formation rates and X-ray selected AGN fractions for the sub-sample of our data with spectroscopy from zCOSMOS (Lilly et al. 2007, 2009). Unless otherwise noted, we use the cosmology $H_0 = 70$ km s^{-1} Mpc^{-1}, $\Omega_m = 0.25$, $\Omega_\Lambda = 0.75$. When referring to other studies, we use units of h_{100}^{-1} kpc where $H_0 = 100$ km s^{-1} Mpc^{-1}. As in Ilbert et al. (2013), magnitudes are given on the AB system (Oke 1974) and stellar masses in units of $M_\odot$ with a Chabrier (2003) IMF.

2. DATA

Finding late-stage galaxies mergers with two intact nuclei out to $z \sim 1$ requires the high resolution available in space-based images. We apply our pair finding method to *HST*/ACS F814W ($I-$band) images taken as part of the COSMOS project (Koekemoer et al. 2007; Massey et al. 2010). The pixel scale in these images in $0.03''$/pixel and the point spread function has a FWHM of ~ 0.09 pixels, which corresponds to 0.6 kpc at redshift $z = 1$. Although our merger-finding method could be applied to ground-based data, it requires that stellar concentrations separated by a few kpc are resolved. In *Sloan Digital Sky Survey* (SDSS) images, the median seeing in $1.3''$, which corresponds to 2.4 kpc at $z = 0.1$. Therefore, our method could only be applied to SDSS data at $z < 0.1$. For ground-based data with better seeing, the redshift limit could be increased to $z \sim 0.3$. However, in order to study the evolution of the merger rate at significant redshift, *HST* data is necessary.

For each galaxy in the parent sample, we create an $8'' \times 8''$ cutout from the ACS F814W image. These cutouts are used for detection of late-stage mergers. For this work we use two, overlapping samples of galaxies, both selected from the COSMOS ACS catalog (Leauthaud et al. 2007). The first sample uses photometric redshifts and contains $\sim 44,000$ galaxies. The second sample includes $\sim 17,000$ galaxies and uses spectroscopic redshifts from the zCOSMOS project (Lilly et al. 2007, 2009). Because of its greater size, we use the photometric sample to study the merger rate as a function of redshift. We use the spectroscopic sample to study the star formation and AGN activity in late-stage mergers.

2.1. *Photometric Redshift Sample*

Our parent galaxy sample is selected from the COSMOS ACS catalog (Leauthaud et al. 2007). We select all objects classified as galaxies (`MU_CLASS` = 1) with total magnitudes brighter than $I = 23$. In the case of a merger, the total magnitude of the post-merger galaxy will be brighter than $I = 23$, while the individual components of the merging galaxy may be up to 5 times fainter ($I \approx 24.7$), but still within the magnitude limit of the COSMOS ACS sample. The magnitude limit is necessary because the completeness of our merger-finding method decreases for lower signal-to-noise (see §3.1). We obtain redshifts and stellar masses for the galaxies in the ACS-selected catalog by matching to the recent K-band selected sample of COSMOS galaxies with photometric redshifts (McCracken et al. 2012; Ilbert et al. 2013). This catalog includes photometric redshifts and stellar masses for 90% of the galaxies in our ACS-selected sample. The missing galaxies are due to slight differences in the area and the masking between the ACS and $K-$band catalogs. We exclude all galaxies masked in Ilbert et al. (2013), as these galaxies do not have reliable photometric redshifts or stellar masses. Ilbert et al. (2013) report a photometric redshift precision of $\sigma_{\Delta z/(1+z)} = 0.008$ for $i^+ < 22.5$. The final sample contains 44164 galaxies.

In §5.2, we study the X-ray selected AGN fraction in late-stage mergers. Therefore, unlike Ilbert et al. (2013), we include known X-ray sources in our parent galaxy sample. For these sources, we use photometric redshifts from Salvato et al. (2011) for optical/NIR sources matched to *XMM* (Brusa et al. 2010) and *Chandra* (Civano et al. 2012) detections. Depending on the type of AGN, these photo-zs are computed using different galaxy-AGN hybrid templates, different luminosity priors, and accounting for source variability. Note that the *Chandra* survey only covers $\sim 1/2$ of the COSMOS area, although at a greater depth. Out of the parent sample of 44164 galaxies, 502 galaxies have an *XMM* counterpart, and 573 have a *Chandra* counterpart, with 282 sources detected by both instruments. For X-ray sources, the photo-zs have a precision of $\sigma_{\Delta z/(1+z)} = 0.015$ (Salvato et al. 2011). For the sources identified in *XMM*, we use stellar masses computed by Bongiorno et al. (2012). These masses and photo-zs are most reliable for galaxies that are not AGN/quasar dominated (type I). For the analysis of the AGN fraction, we will restrict our galaxy sample to systems that are not AGN-dominated, based on the photo-z templates used. This will eliminate galaxies with the least certain photo-zs and stellar masses.

When matching the ACS catalog with the ground-based K-band selected catalog, 1% of sources (640 sources) that are resolved into 2 galaxies in the *HST* data are not resolved in the ground-based data. Clearly, these galaxies are possible late-stage mergers with small separations, and, therefore, cannot simply be removed from the sample. For these cases, we ensure that the galaxy is only included in the sample once, and we use the sum of the I-band magnitudes for the total magnitude. Because our sample is selected from the ACS catalog, we may be missing resolved late-stage mergers in which both of the components are below the $I-$band magnitude limit. However, resolved galaxy pairs make up less than 10% of our final late-stage merger sample, as most of the resolved pairs are more widely separated than the late-stage mergers selected below. From visual inspection, $\sim$ 70% of these resolved galaxy pairs show clear signs of interaction, while the remaining pairs may be chance superpositions. This fraction of chance superpositions agrees well with that obtained by other methods (see §4.1). However, by randomly adding galaxies to COSMOS images, Kampczyk et al. (2007) find the fraction of chance superpositions in a sample of visually-selected mergers is 40% at $z \sim 0.7$, suggesting that visual inspection cannot reliably distinguish real mergers from chance superpositions. Because we use visual inspection to ascertain the number of chance superpositions, we may underestimate the fraction of chance superpositions by almost a factor of two.

For chance superpositions in which two galaxies at different redshifts are unresolved by ground-based observations, the photometric redshifts are especially suspect (Bordoloi et al. 2010). Indeed, in comparing the photometric redshifts to the available spectroscopic redshifts (see §2.2), we find the rate of catastrophic outliers for possible late-stage mergers is 1.6% compared to 1.0% for the entire sample of galaxies between $0.25 < z_{\rm spec.} < 1.0$. However, the catastrophic outlier rate for the late stage merger candidates is still small, and the precision of the photometric redshifts remains unchanged ($\sigma_{\Delta z/(1+{\rm specz})} = 0.004$). In this work, we will assume the photometric redshifts of the late-stage merger candidates are as accurate as those for the entire sample. The comparison to spectroscopic redshifts does not take into account that the spectroscopic redshifts of late-stage mergers may also be suspect, because the galaxies are typically separated by less than an arcsecond and their spectra are blended. We have visually inspected the spectra of late-stage mergers and do not find any in which two merging galaxies are easily discernible in ground-based spectroscopic data.

2.2. *Spectroscopic redshift sample*

In §5, we compare the AGN and star formation rates in our sample of late-stage mergers to kinematically-selected pairs (Kampczyk et al. 2013; Silverman et al. 2011) from the zCOSMOS survey (Lilly et al. 2007, 2009). For the study of SFR (§5.1), we use the bright zCOSMOS 20k bright sample ($I < 22.5$), which contains 16467 galaxies with reliable redshifts. Following Lilly et al. (2009), we only use galaxies with redshifts in the confidence classes: 1.5, 2.4, 2.5, 3.x, 4.x, and 9.5, as well as secondary targets with the same redshift confidences. In principle, the spectroscopic sample should be an exact subset of the larger ACS-selected photo-z sample above. However, differences in masking and the observed region exclude $\sim$ 1200 galaxies in the zCOSMOS survey from the photometric redshift sample described above. Unlike kinematic pair studies in which both members of the merger have measured spectroscopic redshifts, in our sample of late-stage mergers, we only have one spectroscopic measurement for the entire merging system. Most of the late-stage merger candidates described below are separated by less than an arcsecond, so their spectra are blended. As noted above, we have visually inspected a subset of the spectra for these galaxies, and do not find any cases in which two sets of lines (two redshifts) are easily discernible.

In §5.2, we study the fraction of X-ray selected AGN in late stage mergers compared to the fraction of AGN in kinematic pairs. In order to make the comparison straightforward, we use the same parent sample as defined by Silverman et al. (2011) and Kampczyk et al. (2013). As in Silverman et al. (2011), we use *Chandra* observations to identify AGN. Because the *Chandra* survey (Elvis et al. 2009) only covers $\sim 1/2$ of the COSMOS field, the parent sample of galaxies is smaller. Therefore, we only examine 10681 galaxies from the bright zCOSMOS survey which lie within the *Chandra* footprint.

Table 1 lists the various parent samples as well as the their properties. We have also included the cuts made to these samples for the analysis in §4 and §5.

3. MERGING GALAXY SELECTION

To separately detect each component in a merging galaxy, we run the images through a high-pass filter, which makes multiple peaks in the flux distribution easily distinguishable. Our procedure, illustrated in Figure 1, is as follows:

- We first convolve each postage stamp image with a median ring filter (Secker 1995). This smooths the image by replacing each pixel with the median

Table 1
Parent sample properties

Parent sample	$m(I_{814W})$ limit	z limits	$\log M_*/M_\odot$ limit	N_{gal}	N_{merger}	pair sep. limits [kpc]	section
photo-z	< 23	–	–	44164	2047	< 8	§2.1, Table 2[a]
photo-z	< 23	–	–	44164	1547	[2.2,8]	§2.1
photo-z	< 23	[0.25,1.0]	> 10.6	6226	148	[2.2,8]	§4
spec-z	< 22.5	[0.25, 1.05]	> 10.4	5001	166	< 8	§2.2, 5.1
spec-z	< 22.5	[0.25, 1.05]	> 10.4	3474	112	< 8	§2.2, 5.2[b]

[a] The full sample without any cuts in redshift, mass, or pair separation is very incomplete at high redshift. We do not use it for any analysis.
[b] The smaller spectroscopic sample overlaps with the *Chandra* survey (Elvis et al. 2009), which is used to select X-ray AGN.

value in a ring surrounding that pixel, thus erasing structures on scales larger than the ring. We set the inner ring radius to 9 pixels, which is approximately 3 times the PSF width. This sets the size of the smallest separation we can detect. At $z \sim 1.0(0.2)$, 9 pixels corresponds to 2.2(1.1) kpc. For comparison, in SDSS images at $z \sim 0.1$, a 9-pixel radius median ring filter could only detect peaks separated by at least 6 kpc. In order to apply this method to ground-based data, the size of the median ring filter (in pixels) would have to be adjusted for the seeing.

- We then subtract the smoothed image from the original image. Together, the first two steps create a high-pass filter.

- In the difference image, we select all pixels 5 standard deviations above the noise. Contiguous regions are considered a single peak. For a peak detection to be significant, we require a region to contain at least 8 pixels. These values ensure that any detected peak is at least as large as the PSF. We demonstrate in §3.1 that using these detection thresholds yields a sample of peaks which is relatively complete and uncontaminated, particularly for mergers between early-type, bulge-dominated galaxies.

Many of the detections returned by this algorithm are not actually merging galaxies, but rather widely separated galaxies (our postage stamp images span > 50kpc at $z \sim 1$), galaxies with clumpy star formation, spiral arms or bars. Another source of contamination is edge on disk galaxies in which a large bulge is bisected by the dusty disk. In order to eliminate most of these spurious mergers, we place further restrictions on the detected peaks.

First, we require that the peaks are separated by no more than 8 kpc. We use this upper limit to restrict the sample to galaxies that are likely to be mergers, not just close pairs or chance superpositions. Additionally, this eliminates the problem of double-counting late-stage, since widely separated galaxies will be separate detections in the parent galaxy sample.

In order to study the fraction of merging galaxies as a function of redshift, we also implement a lower bound on the peak separation of 2.2 kpc. This lower limit is set by the size of the median ring filter. In this way, we are sensitive to the same mergers at both low and high redshift. Implementing this lower bound on the peak separation eliminates 25% of the late-stage mergers, mainly at low redshift.

Second, we remove detected peaks that are faint compared to the brightest peak in each galaxy *and* to the galaxy as a whole. We measure the flux in each component simply by summing the flux in the pixels associated with the peak. Because this only includes the flux in the central region of each merging component, this is an underestimate of the flux in each component of a merger. Based on merger selection in mock images (see §3.1 and Appendix A), we require that every detected peak contains at least 3% of the the total flux in the galaxy. We demonstrate below that this successfully eliminates $80-90\%$ of the contamination from non-merging galaxies and star-forming clumps, without greatly affecting the completeness of our sample. In order to only study major mergers, we require that every detected peak is at least 1/4 as bright as the brightest peak detected for each galaxy. However, while this cut helps eliminate contamination from minor mergers (see Figure 20), the measured flux ratio is inaccurate as are cuts based on it. Together, the cuts in flux ratio eliminate 75% of the galaxies that would otherwise be considered late-stage mergers. However, neither of these cuts significantly affects our completeness, which is determined by the efficacy of the median ring filter. After these cuts, our overall completeness is $\sim 20\%$, but this increases to $\sim 80\%$ for mergers between bulge-dominated galaxies.

Finally, there are some images that have more than 2 detected peaks. We expect triple merging systems to be extremely rare, and visual inspection shows that most images with 3 or more peaks, after removing faint peaks, are edge-on disk galaxies, in which the bulge and the ends of the spiral arms or bar are detected. These galaxies can be eliminated from the late-stage merger sample by requiring that multiple peaks do not lie along a single line, as is the case for edge-on galaxies. We implement this cut by requiring that the absolute value of the Pearson correlation coefficient for the peak centroids is less than 0.5. After all the other cuts have been applied, this cut eliminates 7% of the detected late-stage mergers (145 of 2047).

With these restrictions, we find 2047 (1547 with separations greater than 2.2 kpc) late-stage mergers with two prominent flux peaks in the photo-z sample of 44164 galaxies. These are listed in Table 2 along with some basic properties of the galaxies and the detected peaks. In the spectroscopic sample of 16467 galaxies, we find 819 merging galaxies, 71 of which are not included in the photo-z sample due to differences in masking. The late-

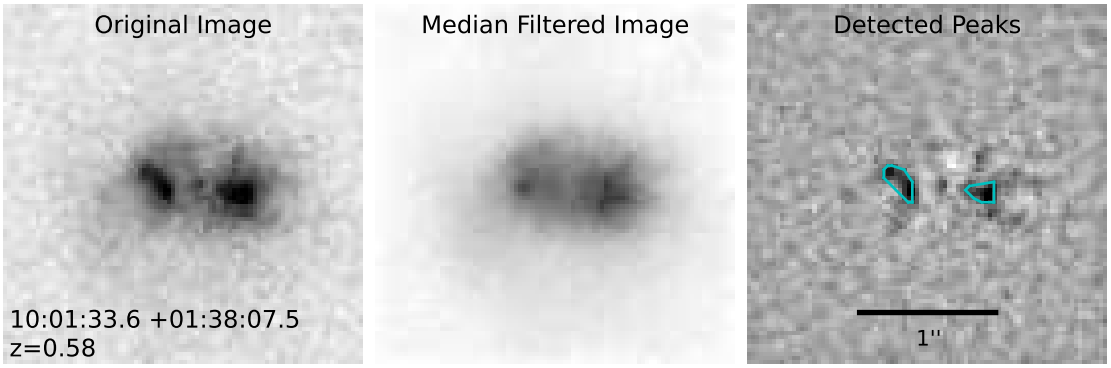

Figure 1. Demonstration of median filter and peak detection on an image of a merger. The (cyan) contours in the last panel outline the two detected peaks in the difference (original − median-filtered) image. The peaks are separated by 4.0 kpc and have a flux ratio of 1:1.

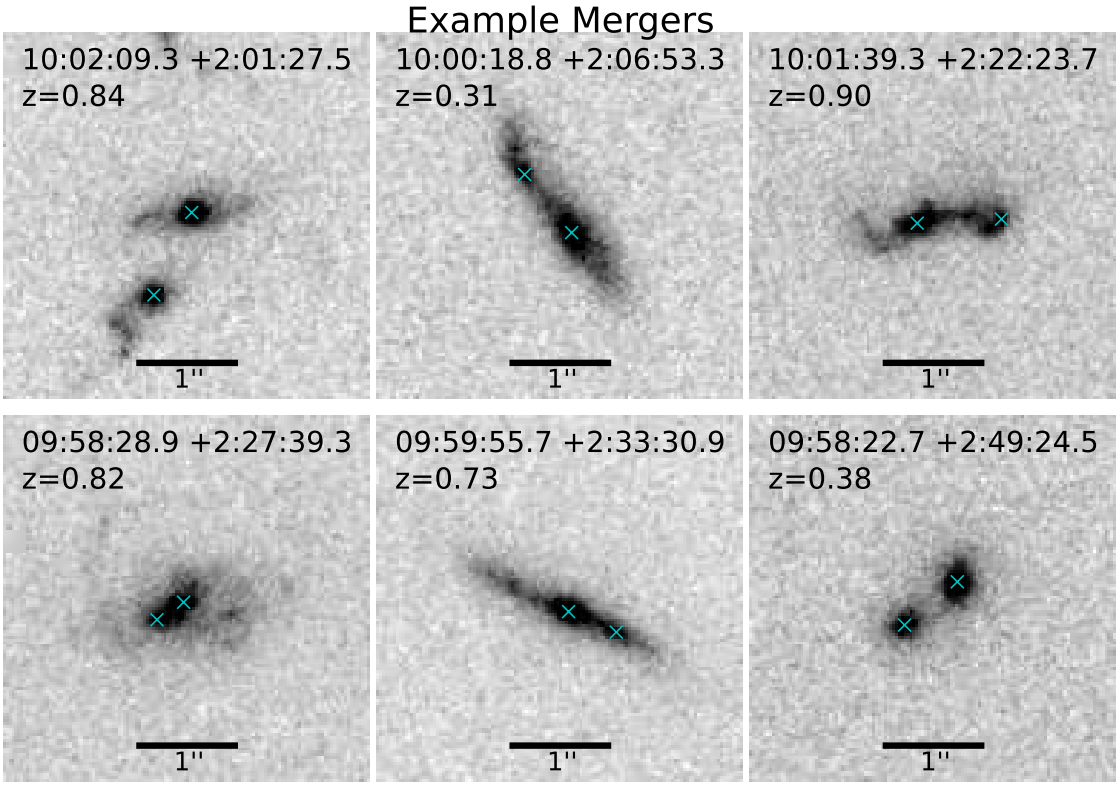

Figure 2. Examples of merging galaxies in the photo-z sample after cuts in peak separation and peak flux. The ×s show peaks found by the median fing filter. The bottom center image may be an edge-on disk with asymmetric spiral arms instead of a merger.

stage mergers in the zCOSMOS sample are also listed in Table 2. For each late-stage merger, we include the projected separation between the two flux peaks as well as the flux ratio of the peaks. In the photo-z sample, 32 mergers are X-ray AGN detected in either *Chandra* or *XMM*. In the spectroscopic redshift sample, 10 late-stage mergers are matched with a *Chandra* source out of 534 mergers that lie within the *Chandra* footprint.

Although we are confident that the majority of late-stage mergers listed in Table 2 are physical late-stage mergers, not all the systems identified by our method will be real mergers. In addition to isolated galaxies with clumpy central structure, our sample contains line-of-sight superpositions. Below, we show these chance superpositions represent 30% of the late-stage merger sample. Without two spectroscopic redshifts for each member of the merger or detailed kinematic maps, it impossible to distinguish real late-stage mergers from widely-separated chance superpositions or from isolated galaxies with complex structures. Indeed, by tuning the selection criteria to accept smaller peaks, our median-ring filter method could be used to find galaxies with several bright clumps instead of late-stage binary mergers.

It is important to note that, other than the pair separation and flux ratio, all other measured properties (e.g., color, redshift, stellar mass, X-ray flux) are properties of the merger, not the individual component galaxies. If we divide galaxies by stellar mass, merging galaxies are counted with galaxies more massive than either member of the merger. In this way, late-stage mergers are treated

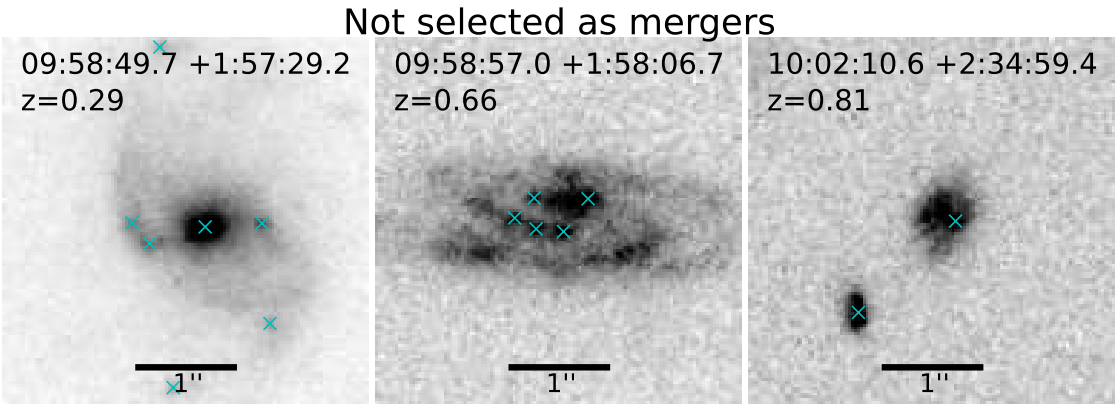

Figure 3. Examples of galaxies with multiple peaks detected, but that are not considered mergers. The ×s show peaks found by the median ring filter. These galaxies are removed from the merger sample by the cuts explained in §3. These galaxies fail because the detected peaks are too faint compared to the central peak (left), all but the central peak are too faint compared to the whole galaxy (middle), and the two peaks have a projected separation larger than 8 kpc (right).

more like post-merger galaxies than like pairs of galaxies in the early stages of merging. This distinction is important to keep in mind when comparing to samples of paired galaxies, in which properties for the individual galaxies are reported.

Figure 2 shows images of 6 late-stage mergers in the photo-z sample. Although the galaxy in the lower middle panel may be a spiral galaxy without any merging activity, the remaining galaxies are clearly mergers at various separations. The typical peak separation is less than $1''$, demonstrating why our algorithm requires the high resolution of space-based data. Figure 3 shows three examples of galaxies which do not satisfy the cuts on peak flux ratio, peak separation, or peak Pearson correlation coefficient. These galaxies are often spiral or barred galaxies. As noted above the median ring filter detects edge-on disk galaxies, in which the bulge is bisected by dust in the disk, as binaries mergers. However, these galaxies represent a small contamination. At fixed star formation rate, the fraction of late-stage mergers candidates is independent of galaxy ellipticity (proxy for disk inclination), suggesting our detection algorithm is not biased by galaxy inclination and dust obscuration.

3.1. *Simulated Merger Images*

We test our merger detection algorithm on a set of simple mock images of merging galaxies. We create postage stamps of pairs of galaxies using the *HST*/ACS images from the photo-z sample. Each mock image contains 2 random galaxies at the same photometric redshift. We choose galaxies at the same redshift in order to eliminate line-of-sight chance superpositions, which we address statistically in §4.1. By using real galaxy images drawn at random, we can create a sample of mergers with realistic morphologies, magnitudes, and flux ratios. Note, however, that this method does not include any structural changes caused by mergers. We simply superimpose images of isolated galaxies.

For each pair of galaxies, we make 8 mock images in which the galaxies are separated by 0.5, 1.5, 2.0, 2.5, 3.0, 5.0, 7.0, and 10.0 kpc. This allows us to test the completeness of our sample as a function of projected separation. Details of the mock images are discussed in Appendix A. Because the flux limits and separation limits used in this study are derived from these simulations, applications of the median-ring filter method to other data sets require new simulations matched to the observations and adjustments to the flux and separation limits given in §3.

After running these mock merger images through the median ring filter, we examine the completeness of our merger sample as a function of pair separation, redshift, and flux ratio. Unsurprisingly, we find that the efficiency of detecting late-stage mergers drops precipitously if the pair separation is smaller than ~ 10 pixels, or the size of the median ring filter (see Figure 18). This motivates using a lower bound of 2.2 kpc (9 pixels at $z \sim 1$) for the pair separation. The median ring filter selects $\sim 40\%$ of the mock mergers with separation larger than 2.2 kpc to $z = 1$. This completeness depends strongly on galaxy morphology. Because the median ring filter smooths away diffuse structures, our merger-finding method is biased toward mergers between concentrated, early-type galaxies[15]. For these mergers, our method is 80% complete, while for mixed mergers (late+early) and mergers between late-type galaxies, the median ring filter only selects 40% of mock mergers. After removing contamination, the completeness of our selection of early-type mergers is independent of redshift. For late-type galaxies, the completeness drops slightly at higher redshifts (see Figure 17, right panel). For all morphologies together, the completeness drops between $z \approx 0.2$ and $z \approx 0.5$, as the fraction of early-type galaxies also decreases toward higher redshift.

In addition to using the mock mergers to study completeness, we can use them to study the contamination from non-merging, clumpy galaxies and minor mergers (see Figure 20). We find that, unlike the completeness, the contamination is essentially independent of redshift. This may reflect the fact that our merger-finding method is less sensitive to all structures at lower signal-to-noise, and, therefore, higher redshift. Using artificially redshifted mergers, Kampczyk et al. (2007) find that mergers identified in low-z data will not appear as mergers at higher redshift due to lower resolution and signal-to-noise, which may explain the incompleteness

[15] We use the ZEST parameter (Scarlata et al. 2007) to ascertain the morphologies of the galaxies in a mock merger. See §3.3 for more details.

Table 2
Late-stage mergers in photo-z + spec-z samples

RA (J2000)[a]	Dec (J2000)[a]	photo-z[b]	spec-z[c]	m_I[d]	$\log M_*/M_\odot$ [e]	separation [″]	flux ratio	*Chand.* $\log L_X$[f]	*XMM* $\log L_X$[f]
149.51058	2.74338	0.49	–	22.21	9.57	0.35	0.50	–	–
149.83214	1.94120	0.66	0.70	22.48	9.50	0.78	0.61	–	–
149.83058	1.90214	0.73	0.73	21.25	10.95	0.62	0.31	42.6	–
150.20693	1.68028	1.11	–	22.76	10.80	0.31	0.88	43.8	43.9
150.39549	2.05754	–	0.96	21.71	10.57	0.44	0.96	43.1	–
150.51472	2.59320	0.37	–	22.71	8.81	0.36	0.34	–	–

Note. — Table 2 is published in its entirety in the electronic edition. A portion is shown here for guidance regarding its form and content.
[a] From Ilbert et al. (2013).
[b] From Ilbert et al. (2013), except for x-ray sources, which are from Salvato et al. (2011).
[c] spectroscopic redshift from zCOSMOS (Lilly et al. 2007, 2009)
[d] *HST*/ACS FW814 AB magnitude from Leauthaud et al. (2007).
[e] Stellar masses for *XMM* sources from Bongiorno et al. (2012); for sources *without* a photo-z, from Bolzonella et al. (2010) and Pozzetti et al. (2010); otherwise, from Ilbert et al. (2013).
[f] $\log L_X$ is the X-ray luminosity in the band $0.5-10$ keV in units of erg s^{-1}. *XMM* data from Brusa et al. (2010), *Chandra* data from Civano et al. (2012).

of our merger selection at high redshift. However, unlike Kampczyk et al. (2007), our merger identification does not take into account morphological k-corrections. Because galaxies are less smooth at bluer wavelengths and have a larger fraction of their flux concentrated in smaller regions, our peak-finding method may detect more non-merging, star forming galaxies at bluer rest frame wavelengths, increasing the contamination. Even if morphological k-corrections are taken into account, galaxies at high redshift are expected to be clumpier (e.g. Bournaud et al. 2007; Genzel et al. 2011) and have higher star formation rates, thus again increasing the contamination from non-merging, clumpy star-forming galaxies. The lack of redshift dependence in the contamination suggests our method is not particularly sensitive to clumpy star-formation at high redshift, possibly because these clumps are too small and faint. A better understanding of the effects of morphological k-corrections will require further study using multi-wavelength data, in particular near-infrared data at $z \sim 1$.

We use the mock mergers to determine the cuts on peak flux to galaxy flux ratio ($> 3\%$) and peak to peak flux ratio ($> 25\%$). By implementing these cuts, we are able to reduce the contamination from non-merging galaxies to 10%, and the contamination from minor mergers (flux ratios smaller than 1:4) to 20%. The median ring filter is naturally less sensitive to minor mergers than major mergers since the faint member of the merger is likely to be below our detection threshold. These cuts do affect the completeness, decreasing it by a factor of 2 to 20% (see Figure 17). However, the completeness for early-type galaxy mergers is larger unaffected. Removing the cut on peak flux to galaxy flux ratio increases the contamination from non-merging sources to $\sim 40\%$, which significantly affects our results on internal late-stage merger properties (SF, AGN), which cannot be simply corrected. In calculating the merger rate (§4), we correct the measured late-stage merger fractions for contamination and incompleteness. For all mergers, we take the contamination to be 30%, independent of redshift. The incompleteness correction is a function of redshift and merger type and is derived from Figure 17.

3.2. *Caveats*

Although our simulations demonstrate the effectiveness of our merger-finding, there are several failure modes of the algorithm. First, the method does not distinguish between merging galaxies and chance superpositions. Since we are looking at extremely small separations, we expect the number of chance superpositions to be small. Although we correct the merger rates in §4 for chance superpositions, we cannot correct the properties of mergers for contamination from chance superpositions.

Second, tests with mock merger images show that the median ring-filter is most sensitive to highly concentrated galaxies. This suggests the merger rate measured for early-type (quiescent) galaxies is very robust, but the merger rate for late-type (star-forming) galaxies is underestimated by as much as a factor of 3, accounting for contamination from non-mergers and line-of-sight superpositions. Furthermore, the bias toward highly concentrated galaxies may introduce biases in the sample as a function of redshift. Morphological k-corrections will lead to more disk-dominated, less centrally concentrated, galaxies at high redshift (Kuchinski et al. 2000; Papovich et al. 2003). Therefore, a bias toward detecting concentrated galaxies is likely to under-report the number of late-stage mergers at high redshift.

Finally, because we impose a flux ratio cut, our method is not sensitive to a merger with only one optically bright AGN. Therefore, in §5.2, we only compute the AGN fraction for obscured (Type II) AGN. Additionally, the stellar masses and photometric redshifts for Type I AGN are less certain than for obscured, optically-faint AGN. Thus, removing Type I AGN from the sample improves the accuracy of our results.

3.3. *Comparison with other selection techniques*

There are many established methods for selecting merging galaxies. The simplest methods select galaxies based on angular separation (e.g., Carlberg et al. 1994; Zepf & Koo 1989). These methods typically look at separations of $5-100\,h_{100}^{-1}$ kpc, and need to be corrected for chance superpositions and galaxies that are physically close, but will not merge within a Hubble time.

The number of superpositions can be limited by requiring the galaxies have similar photometric redshifts (e.g., Kartaltepe et al. 2007; Bundy et al. 2009). Similarly, spectroscopic redshifts are also useful in eliminating chance superpositions (e.g., Patton et al. 2002; Patton & Atfield 2008; Kampczyk et al. 2013; Lin et al. 2004, 2008; Le Fèvre et al. 2000; de Ravel et al. 2009; de Ravel et al. 2011; Ellison et al. 2008). However, spectroscopic samples are limited in size and depth. Furthermore, the late-stage mergers reported here typically have sub-arcsecond separations. Systems with such small separations will not be resolved in ground-based spectroscopic studies, even when including pairs that are observed in the same slit (e.g. Kampczyk et al. 2013). Comparing our results to the spectroscopically-selected pair sample in Kampczyk et al. (2013), we find only 20% of late-stage mergers are also considered kinematic pairs and most of these mergers have separations larger than $2''$.

Pair samples look for galaxies in the early stages of merging. Morphological studies, on the other hand, look for evidence of mergers at all stages, including late-stage mergers and post-merger galaxies. Merger studies based on morphology rely on visual classification (e.g., Kampczyk et al. 2007; Bridge et al. 2010; Darg et al. 2010a; Kartaltepe et al. 2010), or quantitative morphology indicators. Indicators used to distinguish mergers include the Gini coefficient[16] and the second moment of the brightest pixels, M_{20}[17] (e.g., Abraham et al. 2003; Lotz et al. 2004, 2008a); the galaxy asymmetry and concentration (e.g., Conselice et al. 2009; Shi et al. 2009; López-Sanjuan et al. 2009); and combinations of the above as well as parametric fits to galaxy luminosity profiles (e.g., Scarlata et al. 2007; Cassata et al. 2005). In particular, Scarlata et al. (2007) use principle component analysis to reduce the space spanned by Gini, M_{20}, concentration, asymmetry, clumpiness, and galaxy Sérsic index to three dimensions. Regions in this space are then assigned a ZEST (Zurich Estimator of Structural Types) type. This estimator has been applied to the COSMOS ACS images, making comparisons to our late-stage merger sample possible.

Figures 4 and 5 show the ZEST classifications of our sample. All morphological values are taken from Scarlata et al. (2007). As described in Scarlata et al. (2007), the ZEST types are computed based on 'clean' ACS images, in which close companions, if found, are masked. Therefore, we expect that for some mergers, one member of the pair will be masked, decreasing the measured asymmetry and M_{20}. However, inspection of the COSMOS 'clean' images shows that the majority of late stage mergers are considered a single system (see Cisternas et al. 2011). We limit the sample to galaxies with stellar masses above $2.5 \times 10^{10}\,\mathrm{M}_{\odot}$ and $I-$band magnitudes brighter than 23.5. The mass-restricted parent sample is shown by colored contours, while the late-stage mergers are denoted by black points. In these figures, it is clear that most mergers are either ZEST type 2 (bulge+disk galaxies) or ZEST type 3 (irregular). Out of 212 late-stage mergers, 28, 112, and 72 are of types 1, 2, and 3, respectively. If the late-stage merger sample had the same distribution as the parent sample, the expected number of each type would be 50, 152, and 10. These differences in ZEST type distribution are shown in the histograms in Figures 4 and 5.

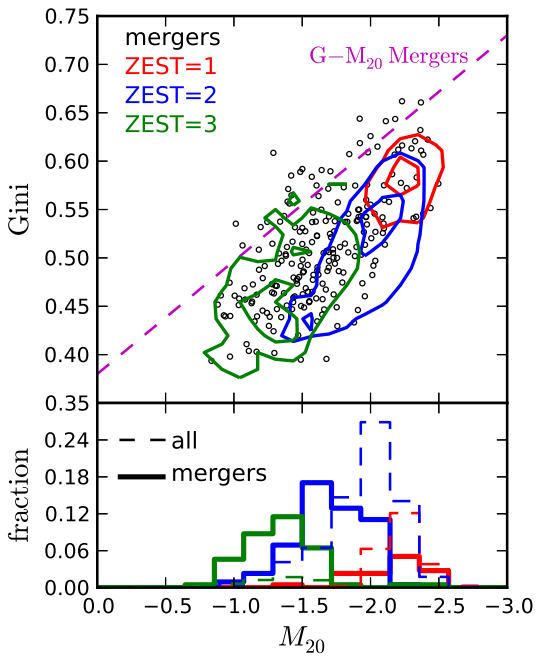

Figure 4. *Top*: Gini coefficient and M_{20} values for late-stage mergers (black points). The contours show the parent sample color-coded by ZEST galaxy type (Scarlata et al. 2007). The sample is limited to galaxies with stellar masses greater than $2.5 \times 10^{10}\,\mathrm{M}_{\odot}$. ZEST=1,2,3 are ellipticals, spirals (with bulges), and irregulars, respectively. The inner(outer) contours contain 30%(80%) of the galaxies of each ZEST type. The dashed magenta line is the criterion for merging galaxies from Lotz et al. (2004). Most late-stage mergers lie below this line and would not be detected using the $G - M_{20}$ method. *Bottom:* Distribution of M_{20} for our sample of mergers (solid lines) and the parent sample (dashed lines). Colors indicate ZEST type as in the top panel.

These histograms show the distributions of M_{20} and concentration for late-stage mergers compared to normal galaxies for each ZEST type. For late-stage mergers classified as spirals, the distribution of M_{20} is shifted toward larger values (blue lines), closer to the distribution for irregular galaxies (green line). This demonstrates that, while the ZEST categorization does not clearly separate late-stage mergers from spiral galaxies, the morphologies of late-stage mergers are measurably different from those of regular spiral galaxies. Nonetheless, most mergers are classified as spirals, in agreement with Kampczyk et al. (2007). Furthermore, most irregular galaxies are not classified as mergers by our method. This is to be expected, since our merger selection only finds major mergers which still have two nuclei, ignoring other merger signatures.

In Figure 4, the magenta dashed line shows the criterion for merging galaxies from Lotz et al. (2004). This criterion is designed for observations in the rest frame

[16] The Gini coefficient measures relative distribution of flux in pixels associated with a galaxy. It is given by $G = 1/\left(2\bar{f}n(n+1)\right)\Sigma_{i=1}^{n}\Sigma_{j=1}^{n}|f_i - f_j|$, where f_i is the flux in a pixel, n is the number of pixels, and $\bar{f}$ is the mean flux per pixel (Abraham et al. 2003)

[17] M_{20} is the second moment of the flux around a galaxy's center ($\Sigma_{i=1}^{n} f_i(x_i^2 + y_i^2)$), only counting the brightest pixels which total 20% of the galaxy's flux. This is then normalized by the galaxy's total second moment, summing over all pixels (Lotz et al. 2004).

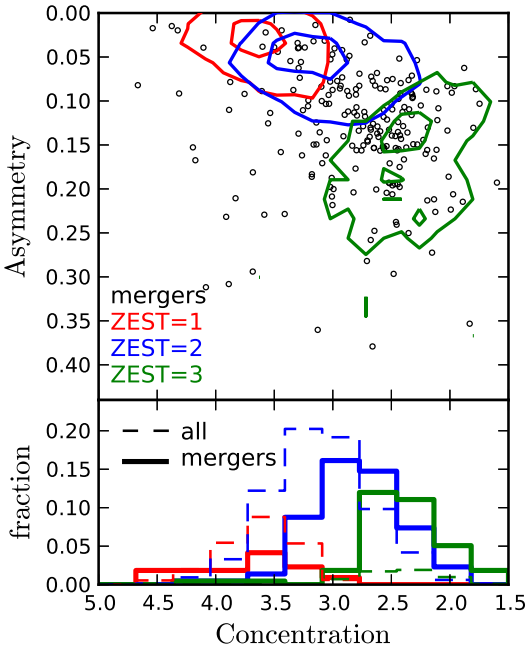

Figure 5. *Top:* Petrosian concentration and asymmetry (about 180° rotation). Symbols and contours are as in Figure 4. Half of the late-stage mergers are of ZEST type 2 (spirals). A late-stage merger is 7 times more likely to be an irregular galaxy (ZEST=3) than a galaxy from the parent sample. *Bottom:* Distribution of concentration for mergers (solid lines) and the parent sample (dashed lines). Colors indicate ZEST type as in the top panel. On average, late-stage mergers of ZEST type 2 (blue lines) are less concentrated than typical ZEST=2 galaxies.

$B-$band and is therefore appropriate for the portion of our sample above $z \approx 0.7$. Objects above this line are considered mergers, However, only a small fraction of late-stage mergers are also mergers based on the G-M_{20} criterion (see also Kartaltepe et al. 2010; Jogee et al. 2009; Lotz et al. 2011). Similarly, in Figure 5, major mergers are expected to be highly asymmetric (asymmetry $\gtrsim 0.3$), but only a small fraction of our sample of late-stage mergers have such high asymmetries.

In Appendix B, we further explore the differences between our sample of late-stage mergers and mergers selected based on their Gini, M_{20}, or asymmetry values. Some differences may be due to the fact that the Gini, M_{20} and asymmetry values reported by Cassata et al. (2005) are based on deblended images, which will split two concentrated nearby galaxies into separated sources. This will eliminate late-stage mergers from the $G - M_{20}$ and asymmetry-selected samples. Furthermore, the high central concentrations of late-stage mergers selected here biases the asymmetry upward, making it less likely they are selected as mergers based on asymmetry. In looking at mergers selected by Gini-M_{20} and asymmetry but *not* by our method, we find that the asymmetry and Gini-M_{20} methods are more sensitive to minor mergers and small perturbations in the galaxy flux distribution than our methods. Together, these reasons help explain the poor overlap between our sample of late-stage mergers and those derived using other morphology methods.

4. MERGER RATES

In section §3.1, we demonstrate the completeness and contamination of our selection of late-stage mergers. By correcting for these effects, we can compute the major merger rate as a function of redshift to $z = 1$. To calculate merger rates, we use the photo-z parent sample, with a few additional restrictions. We restrict our parent sample to the approximately volume-limited sample between $0.25 \leq z < 1.0$ and $\log M_*/\mathrm{M}_\odot > 10.6$. The stellar mass limit is derived by comparing the completeness of our $I-$band selected catalog to that of the deeper $K-$band selected catalog (Ilbert et al. 2013). Up to $z = 1$, 93% of the galaxies from the deeper $K-$band selected catalog are included in our sample. Figure 6 shows the measured stellar masses as a function of apparent magnitude in 3 redshift bins. While the sample is mass-complete for the lower redshift bins, the completeness drops to 82% for $z > 0.9$. For the merger rate analysis, we also remove all sources with X-ray detections because the colors and photometric redshifts for these sources are less certain. This eliminates 3% of the sample. The final sample for the merger rate analysis contains 5894 galaxies, of which 136 are late-stage mergers.

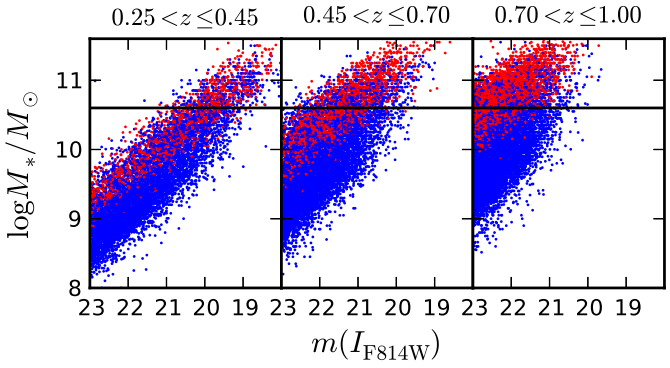

Figure 6. The mass completeness of our photometric sample ($I < 23$) as a function of I_{814W} apparent magnitude in three redshift bins. Quescient(star-forming) (see §4.4) galaxies are shown in red(blue). Up to $z = 0.7$, the sample is complete for both populations. Beyond $z = 0.7$, the completeness drops to $\sim 90\%$, with most of the missing galaxies above $z = 0.9$.

4.1. *Line-of-sight pairs correction*

Before computing the merger rate, we need to correct the observed number of late-stage mergers for chance superpositions. For each galaxy in the sample, we compute the expected number of projected neighbors by summing the average sky density of possible neighbors over the area of the search annulus between 2.2 kpc and 8 kpc. This method is outlined in Bundy et al. (2009). If a galaxy in the parent sample is identified as a merger, it is made of two galaxies with a flux ratio between 1:1 and 1:4. Therefore, for each galaxy the possible companion galaxies are those with fluxes between 1/2 and 1/5 the galaxy's flux. Using the deeper, full ACS source catalog (Leauthaud et al. 2007), we compute the average sky density of possible projected neighbor galaxies. The expected number of chance superpositions for each galaxy is simply the sky density of possible neighbor galaxies multiplied by the area where we search for mergers, namely an annulus with and inner(outer) radius of 2.2 kpc(8 kpc) around each galaxy in the parent sample. Summing the expected number of projected neighbors over the whole parent sample yields an expected number of chance super-positions of 41.4. In other words,

30% of the 136 late-stage mergers are likely to be chance superpositions. Because the angular diameter distance, and, therefore, the size of the annulus searched for close pairs, changes slowly with redshift beyond $z \sim 0.5$, the fraction of chance superpositions does not change significantly with increasing redshift. Therefore, we correct the fraction of late-stage mergers by a factor of $C_{\rm l.o.s.} = 0.7$. This correction is only statistical and does not allow us to determine which late-stage mergers are chance superpositions, only the average probability that any late-stage merger is a spurious pair.

The value of $C_{\rm l.o.s.}$ given above agrees well with the fraction of chance superpositions found by visually inspecting a fraction of the merger images in §2.1. Our correction factor also agrees well with other values for $C_{\rm l.o.s.}$ based on numerical simulations where $C_{\rm l.o.s.} \approx 0.4 - 1.0$ (see Kitzbichler & White 2008; Patton & Atfield 2008; Lotz et al. 2011; Le Fèvre et al. 2000) and visual inspection (Kampczyk et al. 2007). As expected, the fraction of chance superpositions in our sample is smaller than that found by Bundy et al. (2009) using the same method but a larger search annulus. By including photometric redshift information for both members of a merger, Kartaltepe et al. (2007) find a smaller correction factor ($C_{\rm l.o.s.} \sim 15\%$). However, our method cannot distinguish the redshifts of the superimposed galaxies. Despite good agreement with previous studies, the value of $C_{\rm l.o.s.}$ remains highly uncertain and contributes significantly to the uncertainty in the merger rates calculated below.

4.2. *Contamination and completeness*

Using the mock merger images from §3.1, we correct our sample of late-stage mergers for incompleteness and contamination. The simulations show that the sample has a contamination rate of $33 \pm 1\%$, $\sim 20\%$ from minor mergers and $\sim 10\%$ from non-merging, clumpy galaxies. The contamination does not depend strongly on redshift, although it does depend on the flux ratio of the merger. For the merger rate calculation, we correct the number of late-stage mergers for contamination by multiplying by 0.67 ± 0.01.

The simulations also demonstrate the incompleteness of our merger finding method. From Figure 17, the completeness of our sample ranges from $\sim 20\%$ to $\sim 40\%$ as a function of redshift. Based on the mock mergers, we compute the completeness in the three redshift bins used below. The correction factor for incompleteness is simply the inverse of the completeness fraction. In addition to redshift, the completeness of our late-stage merger selection depends strongly on galaxy morphology. In §4.4, we compute the merger rates for star-forming and quiescent galaxies separately. In this case, we use completeness corrections derived from the late-type and early-type galaxy mergers, respectively. While obtaining correct morphologies for artificially superimposed galaxies is trivial, obtaining correct colors requires understanding how the components of the mock merger extinct each other. Instead, we assume that the color (star formation rate) of a merger and the morphology of the merging galaxies are exactly correlated, i.e., there are no star-forming early-type mergers. This is certainly not true, but is likely a small error in light of the overall uncertainties in the corrections for incompleteness and line-of-sight chance superpositions.

Taken with the line-of-sight pair correction, we correct the number of late-stage mergers by three factors, $C_{\rm l.o.s.}$, the contamination (0.67 ± 0.01), and the incompleteness 1/completeness fraction. Together, we denote these corrections as $C_{\rm merge}$. The values of $C_{\rm merge}$ are given in Table 3 along with the *corrected* merger fraction $f_{\rm merge}$. The errors on $C_{\rm merge}$ are the bootstrap-derived errors on the completeness and contamination fractions (see Appendix A) and do not include the uncertainty in $C_{\rm l.o.s.}$. The redshift dependence of $C_{\rm merge}$ is due entirely to the incompleteness correction. In §4.5, we examine the measured merger rate without corrections for incompleteness and contamination in order to determine how sensitive our results are to these correction factors.

4.3. *Evolution of the merger rate*

In order to calculate the merger rate, we simply count the number of pairs in three redshift bins, chosen such that each redshift bin spans the same amount of time. Our results are unchanged if the bins are chosen such that they contain the same number of galaxies. The raw merger fractions are corrected for chance superpositions, contamination, and incompleteness using the correction factor, $C_{\rm merge}$, given in Table 3. The corrected merger fraction for our total sample is $C_{\rm merge} \times 136/5894 = 4.8 \pm 0.5\%$, where $C_{\rm merge} = 2.1 \pm 0.1$, and the completeness fraction is 0.22 ± 0.01. This is comparable to the typical pair fraction found in studies of more widely separated pairs (Lin et al. 2004; Kartaltepe et al. 2007; de Ravel et al. 2009; Bundy et al. 2009; Robaina et al. 2010). and the fraction of morphologically disrupted systems (De Propris et al. 2007; Conselice et al. 2009; Lotz et al. 2008a). As noted in §3.3, our sample of late-stage mergers has little overlap with samples of major mergers selected by visual inspection or other non-parametric methods (asymmetry, etc.). This makes the remarkably good agreement in the overall fraction of mergers difficult to interpret, and possibly due to chance.

In order to compute the galaxy merger rate, we must take into account the timescale over which a late-stage merger could be observed. We calculate the fractional merger rate as it is defined in (Lotz et al. 2011):

$$\Re_{\rm merge} = f_{\rm merge} \langle \frac{1}{T_{\rm obs}} \rangle \, , \qquad (1)$$

where $T_{\rm obs}$ is the duration of time a merger will be observable. Because $T_{\rm obs}$ is highly dependent on the merger/pair selection, using the correct value for $T_{\rm obs}$ is essential when comparing merger rates based on different techniques (see Lotz et al. 2011). For the late-stage mergers studied here, $T_{\rm obs}$ is sensitive to many parameters such as the galaxy masses, gas fractions, orbital parameters, and observational angle. Many pair studies use the dynamical friction timescale for $T_{\rm obs}$ (Lin et al. 2004; Bell et al. 2006; Patton & Atfield 2008; Masjedi et al. 2008). Another way to determine $T_{\rm obs}$ is using hydrodynamical simulations of galaxy mergers and directly measuring how long close pairs or morphological signatures are observable (e.g., Patton et al. 2000; Conselice 2006; Kitzbichler & White 2008; Lotz et al. 2008b, 2010a,b, 2011). For close pairs separated by $5 - 20\, h_{100}^{-1}$ kpc, Lotz et al. (2011) find $\langle T_{\rm obs} \rangle \approx 0.33$ Gyr,

Table 3
Pair fractions and merger rates

z	$N_{\rm gal}$	$N_{\rm mgr}$	$C_{\rm merge}$	$f_{\rm merge}$	$\Re\,[{\rm Gyr}^{-1}]$
[0.25, 0.45)	867	15	1.1 ± 0.1	$1.9 \pm 0.5\%$	$5.9 \pm 1.6\%$
[0.45, 0.70)	1644	39	1.8 ± 0.1	$4.2 \pm 0.8\%$	$12.6 \pm 2.3\%$
[0.70, 1.00)	3383	82	2.7 ± 0.1	$6.6 \pm 0.8\%$	$20.1 \pm 2.5\%$
low mass ($10.6 < \log M/{\rm M}_\odot < 10.9$) sample					
[0.25, 0.45)	399	9	1.1 ± 0.1	$2.5 \pm 0.9\%$	$7.7 \pm 2.6\%$
[0.45, 0.70)	782	23	1.8 ± 0.1	$5.1 \pm 1.2\%$	$15.6 \pm 3.5\%$
[0.70, 1.00)	1766	42	2.7 ± 0.1	$6.5 \pm 1.1\%$	$19.7 \pm 3.2\%$
high mass ($\log M/{\rm M}_\odot \geq 10.9$) sample					
[0.25, 0.45)	468	6	1.1 ± 0.1	$1.4 \pm 0.6\%$	$4.4 \pm 1.8\%$
[0.45, 0.70)	862	16	1.8 ± 0.1	$3.2 \pm 0.9\%$	$9.8 \pm 2.6\%$
[0.70, 1.00)	1617	40	2.7 ± 0.1	$6.8 \pm 1.1\%$	$20.5 \pm 3.4\%$
star-forming sample					
[0.25, 0.45)	413	8	1.4 ± 0.2	$2.7 \pm 1.1\%$	$8.2 \pm 3.2\%$
[0.45, 0.70)	763	21	2.0 ± 0.2	$5.6 \pm 1.4\%$	$16.9 \pm 4.1\%$
[0.70, 1.00)	1131	36	3.4 ± 0.3	$10.7 \pm 2.0\%$	$32.4 \pm 6.1\%$
quiescent sample					
[0.25, 0.45)	454	7	0.6 ± 0.0	$0.9 \pm 0.3\%$	$2.6 \pm 1.0\%$
[0.45, 0.70)	881	18	0.6 ± 0.0	$1.1 \pm 0.3\%$	$3.5 \pm 0.8\%$
[0.70, 1.00)	2252	46	0.6 ± 0.0	$1.3 \pm 0.2\%$	$3.9 \pm 0.6\%$
star-forming, low mass ($10.6 < \log M/{\rm M}_\odot < 10.9$) sample					
[0.25, 0.45)	225	4	1.4 ± 0.2	$2.5 \pm 1.3\%$	$7.5 \pm 4.0\%$
[0.45, 0.70)	469	10	2.0 ± 0.2	$4.3 \pm 1.5\%$	$13.1 \pm 4.4\%$
[0.70, 1.00)	660	22	3.4 ± 0.3	$11.2 \pm 2.6\%$	$33.9 \pm 7.9\%$
quiescent, low mass ($10.6 < \log M/{\rm M}_\odot < 10.9$) sample					
[0.25, 0.45)	243	2	0.6 ± 0.0	$0.5 \pm 0.3\%$	$1.4 \pm 1.0\%$
[0.45, 0.70)	393	6	0.6 ± 0.0	$0.9 \pm 0.4\%$	$2.6 \pm 1.1\%$
[0.70, 1.00)	957	18	0.6 ± 0.0	$1.2 \pm 0.3\%$	$3.6 \pm 0.9\%$
star-forming, high mass ($\log M/{\rm M}_\odot \geq 10.9$) sample					
[0.25, 0.45)	188	4	1.4 ± 0.2	$3.0 \pm 1.6\%$	$9.0 \pm 4.8\%$
[0.45, 0.70)	294	11	2.0 ± 0.2	$7.6 \pm 2.5\%$	$23.0 \pm 7.5\%$
[0.70, 1.00)	471	14	3.4 ± 0.3	$10.0 \pm 2.8\%$	$30.3 \pm 8.6\%$
quiescent, high mass ($\log M/{\rm M}_\odot \geq 10.9$) sample					
[0.25, 0.45)	211	5	0.6 ± 0.0	$1.3 \pm 0.6\%$	$4.0 \pm 1.8\%$
[0.45, 0.70)	488	12	0.6 ± 0.0	$1.4 \pm 0.4\%$	$4.2 \pm 1.2\%$
[0.70, 1.00)	1295	28	0.6 ± 0.0	$1.4 \pm 0.3\%$	$4.1 \pm 0.8\%$

Note. — The fraction of mergers is corrected by a factor of $C_{\rm merge}$ for line-of-sight superpositions, contamination from minor mergers/non-mergers, and incompleteness. The fractional merger rate is calculated using $\langle T_{\rm obs} \rangle = 0.33$ (Lotz et al. 2011).

and that $\langle T_{\rm obs} \rangle$ is essentially independent of galaxy gas fraction, and, therefore, redshift. Therefore, $T_{\rm obs}$ only affects the normalization of the merger rate, not the slope as a function of redshift. Below, we use the merger observation timescale computed by Lotz et al. (2011), $\langle T_{\rm obs} \rangle = 0.33$ Gyr. This is roughly 2× longer than the *minimum* expected $T_{\rm obs}$, namely the orbital timescale. For mergers with masses near the Milky Way mass, separated by 8 kpc, the orbital timescale is ~ 0.2 *Gyr*. Nonetheless, the value of $T_{\rm obs}$ introduces significant uncertainty in the normalization of the merger rate. Using $\langle T_{\rm obs} \rangle = 0.33$, the computed values for $\Re_{\rm merge}$ are reported in the last column in Table 3.

Based on the corrected fraction of late-stage mergers,

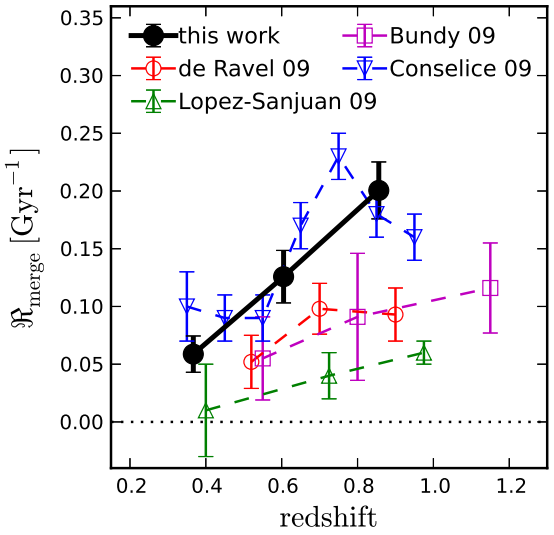

Figure 7. The fractional merger rate as a function of redshift derived from our sample of late-stage mergers (black, filled circles), compared to other stellar mass-selected studies of merging galaxies. Bundy et al. (2009) and de Ravel et al. (2009) identify merging galaxies as photometric pairs. López-Sanjuan et al. (2009); Conselice et al. (2009) identify mergers based on galaxy asymmetry. All data is from Lotz et al. (2011) in which the timescales for observation of mergers are calibrated to facilitate easy comparison. Our merger rates are corrected from line-of-sight superpositions, contamination and incompleteness. The error bars on our points (black) are the statistical error bars only, but include the uncertainties in the correction for contamination and incompleteness.

we find $\Re_{\rm merge} \propto (1+z)^{3.8 \pm 0.9}$, consistent with, albeit slightly steeper than, results of other studies that find significant evolution in the merger rate with redshift (de Ravel et al. 2009; Lin et al. 2008; Robaina et al. 2010, but see Bundy et al. 2009; Lotz et al. 2011). The merger rate is also consistent with the expected merger rate for dark matter halos, which grow as $(1+z)^{3-4}$ (e.g., Fakhouri et al. 2010, but see Berrier et al. 2006; Guo & White 2008). This suggests that, at late times, massive galaxy growth traces halo growth. Figure 7 shows the fractional merger rate for late-stage mergers compared to other merger rate studies, including studies using close pairs (de Ravel et al. 2009; Bundy et al. 2009) and galaxy asymmetry (López-Sanjuan et al. 2009; Conselice et al. 2009). The values plotted are from Lotz et al. (2011) and take into account differences in $T_{\rm obs}$ for different merger-finding methods.

Because the measured merger rate evolution depends on galaxy selection (Lotz et al. 2011), we limit the comparison to other mass-selected samples. All four studies in Figure 7 use mass-selected samples, with mass limits near $\log M_*/{\rm M}_\odot \gtrsim 10$, lower than our mass limit. Additionally, for the pair studies, the mass refers to the mass of the individual merging galaxies, *n*ot the final merged galaxy, as is the case in our study. Therefore, care must be taken when comparing these results. Nonetheless, the agreement between the different methods suggests that above $\log M_*/{\rm M}_\odot \sim 10$, the merger rate does not depend strongly on galaxy mass. However, the errors on $\Re_{\rm merge}$ are statistical errors only and do not include uncertainties in $T_{\rm obs}$. A smaller value for $T_{\rm obs}$ will increase the measured $\Re_{\rm merge}$, and lessen the agreement between our study and previous results.

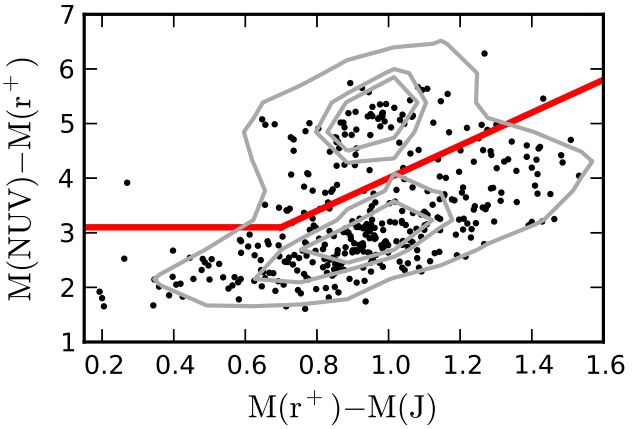

Figure 8. Color-color diagram for selecting queiscent and star-forming galaxies. The cuts are from Ilbert et al. (2013, 2010). Queiscent galaxies are in the upper left. The data shown is in the redshift range $0.25 < z < 1.0$ and with stellar masses $> 10^{10}\mathrm{M}_{\odot}$. The contours show the distribution of the full photo-z sample, with contours at the 30^{th}, 50^{th}, and 90^{th} percentiles. The points show the late-stage mergers.

4.4. *Mergers as a function of color and stellar mass*

Because our sample of late-stage mergers is relatively large, we can explore the evolution of the merger rate as a function of color and stellar mass. We divide the parent sample into two mass bins, choosing the median stellar mass, $\log M/\mathrm{M}_{\odot} = 10.9$ as the division. Following Ilbert et al. (2013), we further divide the sample into quiescent and star-forming galaxies, based on the rest frame near-UV (NUV)$-r^{+}$ and $r^{+} - J$ colors, where NUV corresponds to the GALEX filter at $0.23\,\mu$m, and r^{+} refers to the Subaru $r-$band. Colors are computed from the best-fit SED templates in Ilbert et al. (2013). The color cuts for quiescent galaxies are: $(\mathrm{NUV} - r^{+}) > 3(r^{+} - J) + 1$ and $(\mathrm{NUV} - r^{+}) > 3.1$ (Ilbert et al. 2013, 2010). The color-color diagram in Figure 8 shows these cuts applied to our sample.Our analysis cannot distinguish the colors of the member galaxies in a late-stage merger. Nonetheless, we classify mergers as 'wet' (gas-rich) mergers if the total merging system is star-forming, as 'dry' mergers if the merger is quiescent.

Table 3 contains the corrected pair fractions within each star-forming/stellar mass bin. The fractions and merger rates reported are those within the limited star-forming/stellar mass parent sample. Note that we use the same T_{obs} for all sub-samples of galaxies, even though T_{obs}will likely to depend on the galaxy masses and color. Within a single sub-population, however, T_{obs} does not depend strongly on redshift, and, therefore, does not affect the evolution of the merger rate, only the normalization. The pair fractions reported in Table 3 are corrected for incompleteness and contamination. In addition to a dependence on redshift, C_{merge} is different for quiescent and star-forming galaxies because the completeness of our merger selection depends on galaxy morphology, and, therefore, color. For quiescent galaxies, we use the completeness fraction for early-type galaxies, while for star-forming galaxies, we assume the completeness of late-type mergers. For quiescent galaxies, C_{merge} is independent of redshift, while, for star-forming galaxies, C_{merge} increases by a factor of ~ 2 from $z \approx 0.2$ to $z \approx 1.0$ (see §4.5).

Figure 9 shows the corrected pair fractions for each subsample of galaxies as a function of redshift. From these figures it is evident that the merger rates for blue and red galaxies are significantly different. For blue galaxies $\Re_{\mathrm{merge}} \sim (1+z)^{4.5\pm1.3}$, while for red galaxies $\Re_{\mathrm{merge}}$ is consistent with no evolution, $\Re_{\mathrm{merge}} \sim (1+z)^{1.1\pm1.2}$. This suggests that the evolution in the merger rate for *all* galaxies is driven by the evolution in the merger rate for blue galaxies and the increasing contribution of blue galaxies to the galaxy population at high redshift.

For massive ($\log M/\mathrm{M}_{\odot} > 10.9$), quiescent galaxies, $\Re_{\mathrm{merge}} \sim (1+z)^{0.0\pm1.4}$, consistent with no evolution. The lack of evolution in the merger rate for massive, red galaxies agrees with results from pair studies (de Ravel et al. 2009; de Ravel et al. 2011; Lin et al. 2008; Bundy et al. 2009; López-Sanjuan et al. 2011, 2012) and simulations (Kitzbichler & White 2008). As in Lin et al. (2008), de Ravel et al. (2009) and Darg et al. (2010b), we find that most mergers are star-forming, and that the fraction of star-forming mergers increases significantly with redshift. Figure 10 shows that dry, quiescent mergers mergers make up $\sim 20\%$ of all mergers in our sample, once the merger fractions are corrected for incompleteness and contamination.

It is interesting to note that Figure 9 shows a weak increase in the fractional merger rate for low mass, quiescent galaxies ($\Re_{\mathrm{merge}} \propto (1+z)^{3.0\pm2.2}$). However, low-mass quiescent galaxies suffer the most from incompleteness in this $I-$band selected sample. If the average stellar mass for low mass quiescent galaxies increases as a function of redshift, then it is not surprising that the fractional merger rate in the highest redshift bin matches that of the high-mass quiescent galaxies. This suggests the evolution the low mass quiescent galaxy merger rate may be a selection effect.

The fractional merger rate for star-forming galaxies grows significantly with increasing redshift, $\Re_{\mathrm{merge}} \propto (1+z)^{3.5\pm1.8}$ for high mass galaxies, and $\Re_{\mathrm{merge}} \propto (1+z)^{5.4\pm1.7}$ for low mass galaxies. This demonstrates the increasing importance of wet major mergers at high redshift, in agreement with previous studies (Li et al. 2008; Bundy et al. 2009; López-Sanjuan et al. 2012, 2011). The strongly increasing fraction of star-forming mergers also agrees with the increase in bright infrared sources as a function of redshift (Le Floc'h et al. 2005). This is expected as these sources are often associated with mergers (Sanders & Mirabel 1996; Kartaltepe et al. 2010).

As with quiescent galaxies, the merger rate evolution for low mass galaxies is steeper than for high mass galaxies. Although this may be driven by incompleteness, the steepness of the merger rate for lower mass galaxies suggests a dependence of the merger rate on halo mass. Note, however, that the range of masses under study is small ($10.6 \leq \log M/\mathrm{M}_{\odot} \lesssim 11$). The differences in $\Re_{\mathrm{merge}}$ for samples of star-forming, quiescent, low mass and high mass galaxies help explain the differences in merger rates found using different parent samples, especially the differences in $\Re_{\mathrm{merge}}$ between mass-limited and luminosity-limited samples (e.g., Lotz et al. 2011; Lin et al. 2004).

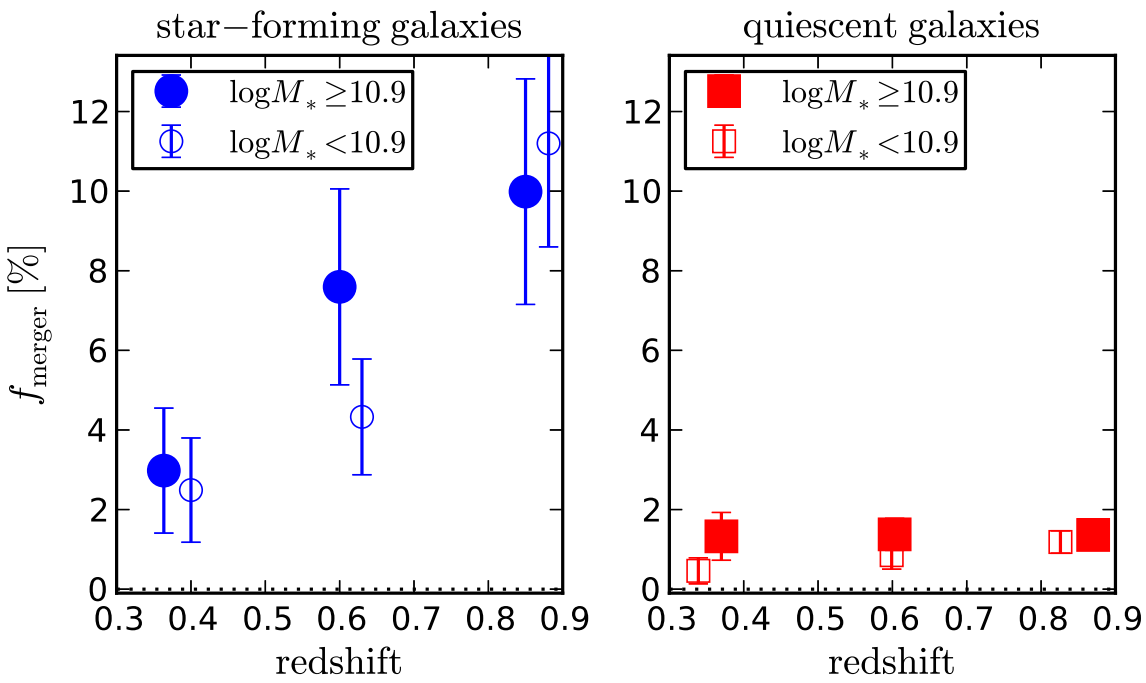

Figure 9. The fraction of mergers for different types of galaxies, corrected for chance line-of-sight superpositions, contamination, and incompleteness, as a function of redshift. The left panel shows star-forming galaxies while the right panel shows queiscent galaxies, separated by the color cuts in Figure 8. The solid (empty) symbols show high (low) mass galaxies. Small horizontal offsets are added for visibility.

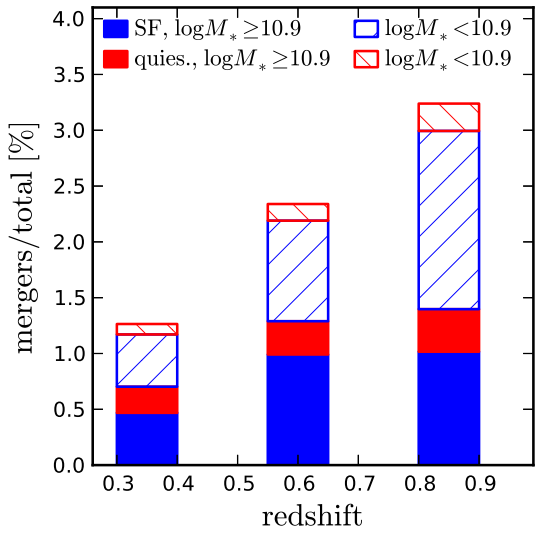

Figure 10. The fraction of pairs split by galaxy color and mass, corrected for line-of-sight superpositions, incompleteness and contamination. With these corrections, mergers between star-forming galaxies dominant at all redshifts, and the number of star-forming mergers increases significantly with redshift.

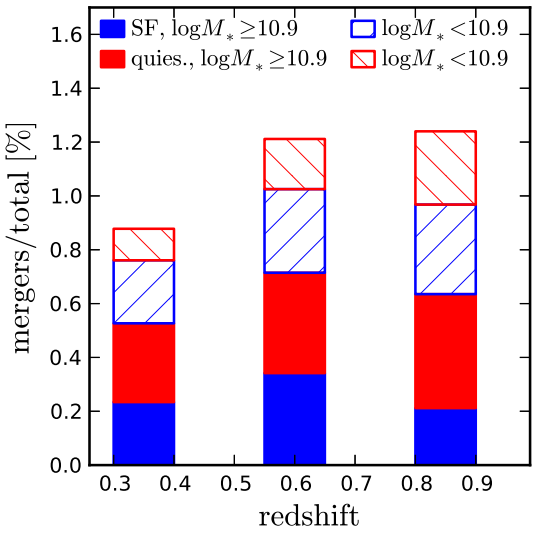

Figure 11. As in Figure 10, but the fractions are *not* corrected for incompleteness or contamination. Without the incompleteness corrections, there is no statistically significant increase in merger activity at high redshifts. Because the correction factor is small for early-type galaxies, the fraction of queiscent mergers is nearly the same as in Figure 10.

4.5. *Without incompleteness/contamination corrections*

The results in Figures 7 through 10 use late-stage merger fractions corrected for incompleteness and contamination. While these correction factors are based on simulations well-matched to the observed data, the corrections are still uncertain. Therefore, we perform the same analysis, excluding the completeness and contamination corrections, setting $C_{\rm merge} = 0.7$ for the line-of-sight pairs correction. This only serves to demonstrate the effect of our correction factors. The simulations clearly demonstrate the need for incompleteness and contamination corrections, and the measured merger rates are certainly invalid without any corrections. Without the incompleteness corrections, the overall late-stage merger fraction drops by a factor of ~ 2. Furthermore, the measured evolution in the merger rate disappears if we do not include an evolving correction for incompleteness. Figure 11 demonstrates that the fraction of late-stage mergers only evolves slightly with redshift, $f_{\rm merge} \propto (1+z)^{0.8\pm0.8}$ This is in contrast to Figure 10, which shows a large increase in the *corrected* merger frac-

tion with redshift.

Comparing Figures 10 and 11 also shows that the fraction of quiescent mergers is unchanged by the correction factor for contamination and incompleteness. This is unsurprising since our merger sample is complete for early-type galaxies out to $z \sim 1$. The completeness correction mainly affects star-forming galaxies, particularly at high redshift. Without corrections for contamination and incompleteness, the merger rates for quiescent and star-forming galaxies grow as $\Re_{\rm merge} \propto (1+z)^{0.7\pm1.2}$ and $\Re_{\rm merge} \propto (1+z)^{1.5\pm1.2}$, respectively. While the merger rate evolution for quiescent galaxies is unchanged, the merger rate for star-forming galaxies is significantly lower, and only marginally inconsistent with a flat merger rate. These results suggest that the non-evolving merger rate for quiescent galaxies is robust. For star-forming galaxies, the uncorrected merger rates represent a lower limit. Even if the exact values of the incompleteness we measure using mock merger images are inaccurate, our sample of late-stage mergers is demonstrably incomplete at high redshift, particularly for late-type, star-forming galaxies. Therefore, the merger rate for star-forming galaxies will evolve at least as quickly as $(1+z)^{1.5\pm1.2}$.

In the above analysis, we use a contamination correction that is independent of redshift and galaxy type (quiescent or star-forming). However, there are several contamination effects which are likely larger for star-forming galaxies than for quiescent galaxies. These contaminants may artificially boost the late-stage merger fraction at high redshift. Correcting for these effects will lower the merger rate evolution rate. The star-forming galaxy merger rate is particular sensitive to morphological k-corrections and the overall increase in the fraction of clumpy, star-forming galaxies at high redshift. This increase in the contamination will lead to an artificial increase in the merger rate for star-forming galaxies at high redshift. However, as demonstrated in §4.1 and Appendix A, the overall contamination rate from non-merging galaxies is $\sim 10\%$, while the completeness is only $\sim 20\%$, and the former only depends weakly on redshift. Therefore, we expect the effects of incompleteness to dominate over any effects from contamination, and the results presented above to be robust, despite the large correction for incompleteness and contamination.

5. PROPERTIES OF LATE-STAGE MERGERS

To study the internal properties of late-stage mergers, we limit our parent sample to galaxies from the spectroscopic zCOSMOS survey (Lilly et al. 2007, 2009). The 'bright' zCOSMOS sample contains spectra for $\sim 20,000$ galaxies ($I < 22.5$). The zCOSMOS sample should be a subsample of the K-band selected sample from Ilbert et al. (2013) described above, but differences in masking mean that some zCOSMOS galaxies are missing from the photo-z sample. To ensure no galaxies are missing, we rerun our merger selection algorithm on postage stamps generated from the zCOSMOS parent sample. The final sample is selected in the same way as that used in Kampczyk et al. (2013) and Silverman et al. (2011) to study the SFRs and AGN properties of kinematic pairs. Below, we compare the properties of late-stage mergers both to the parent zCOSMOS sample and to more widely separated kinematic pairs from the same parent sample.

Because these galaxies are observed in zCOSMOS, we use the spectroscopic redshifts, and stellar masses from Pozzetti et al. (2010) and Bolzonella et al. (2010). These stellar masses use the spectroscopic redshifts and are in good agreement with those measured in Ilbert et al. (2013) using photometric redshifts. For the analysis below, we examine galaxies with $M_* > 2.5\times10^{10}{\rm M}_\odot$ in the redshift range $0.25 \le z < 1.05$, the same mass and redshift range used in kinematic pair studies in zCOSMOS (Silverman et al. 2011; Kampczyk et al. 2013). For the analysis of the SFR (§5.1), we remove all sources with a *Chandra* or *XMM* detection. This leaves a sample of 4586 galaxies of which 154 are classified as late-stage mergers. We use the non-merging galaxies from the parent zCOSMOS sample as a control sample. However, we first check that the control sample is well-matched to the merger sample in stellar mass and redshift. Since AGN activity, SFR and, in this sample of galaxies, sSFR (see Maier et al. 2009), are strong functions of M_* and z, it is important that the late-stage merger sample is not biased relative to the control sample. Kolmogorov-Smirnov (K-S) tests show that both the mass and redshift distributions for late-stage mergers and the control sample are indistinguishable.

5.1. *Star formation in late-stage mergers*

Simulations show that galaxy mergers lead to enhanced star formation (e.g., Hernquist 1989; Di Matteo et al. 2007; Mihos & Hernquist 1996; Barnes & Hernquist 1991; Springel et al. 2005; Hopkins et al. 2006). There is also much observational evidence to support this conclusion. Galaxies identified as mergers are often bluer (e.g., Kampczyk et al. 2007; Darg et al. 2010a) and show enhanced UV and IR SFR (e.g., Jogee et al. 2009; Robaina et al. 2009). Spectroscopy confirms that galaxies in close pairs have higher star formation rates than isolated galaxies (e.g., Barton et al. 2000; Lambas et al. 2003; Kampczyk et al. 2013; Ellison et al. 2013). Studies of far-infrared selected galaxies show that galaxies with very high star formation rates are much more likely to be disturbed morphologically than galaxies with typical star formation rates (e.g., Sanders & Mirabel 1996; Kartaltepe et al. 2010). In this section, we compare the SFR in late-stage mergers to that of isolated galaxies. Our control sample of isolated galaxies is simply the set of zCOSMOS galaxies that are not identified as late-stage merger candidates.

Figure 12 shows the narrow 4000-Angstrom break (Balogh et al. 1999) for late stage mergers and the control sample. As expected, at fixed stellar mass, the late-stage mergers have a lower median $D_n(4000)$ than the control sample. This is indicative of recent, within the last Gyr, star formation in the late stage mergers. A K-S test shows that the distributions of $D_n(4000)$ for the late-stage mergers and the control sample are distinct. Indeed, at masses below $\log M/{\rm M}_\odot = 10.7$, there are almost no quiescent late-stage mergers. This indicates that a significant fraction of star formation may be associated with mergers.

We use the SFR computed from the 24μm flux as measured by *Spitzer/MIPS* (Sanders et al. 2007; Le Floc'h et al. 2009). The total infrared luminosity, $L_{\rm IR}$ is computed using the spectral energy distribution models from Dale & Helou (2002) and the photometric redshifts from Ilbert et al. (2009) and Salvato et al. (2009)

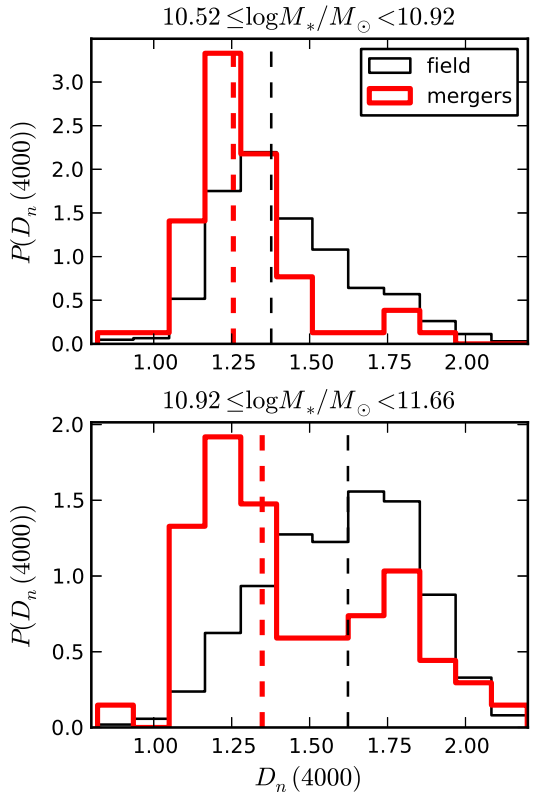

Figure 12. The distribution of the narrow 4000 Å-break for late-stage mergers (red) and the parent sample (black) from zCOSMOS. The galaxies are divided into two mass bins. In the upper(lower) panel there are 1582(2375) control galaxies and 69(67) merging galaxies. The corresponding vertical lines show the medians of each distribution. The median $D_n(4000)$ for late-stage mergers is smaller in both mass bins, indicating most late-stage mergers have undergone recent star formation.

for X-ray sources. Below $z \sim 1$, the 24μm flux is an accurate measure of the total infrared luminosity (e.g., Elbaz et al. 2010). From the infrared luminosity, the total SFR is given by Kennicutt (1998):

$$\mathrm{SFR}\ [\mathrm{M}_\odot\ \mathrm{yr}^{-1}] = 4.5 \times 10^{-44} L_{\mathrm{IR}}/L_\odot\,. \qquad (2)$$

We only utilize sources with a 24μm-detection and a measured SFR. This limits our sample to 2318 galaxies, of which 111 are late-stage mergers. Among galaxies with non-zero 24μm-based SFRs, the fraction of late-stage mergers is $4.8 \pm 0.5\%$; in the full zCOSMOS sample, the fraction of late-stage mergers is $3.3 \pm 0.3\%$, suggesting an enhancement in the average SFR in late-stage mergers.

Figure 13 shows the cumulative distributions of the specific star formation rate (sSFR) for our sample of mergers and galaxies in the control sample. The sSFR is calculated from the 24μm-based SFR and the stellar mass from Pozzetti et al. (2010). The measured stellar mass is increased by a factor 1.8 to account for the difference in initial mass function (IMF). Pozzetti et al. (2010) use a Chabrier IMF while the SFR is computed assuming a Salpeter IMF (Kennicutt 1998). Figure 13 shows that the distribution of sSFR is skewed to higher values for mergers compared to other galaxies in the parent sample. A K-S test shows the two distributions of sSFR are distinct. The median sSFR in late-stage mergers is

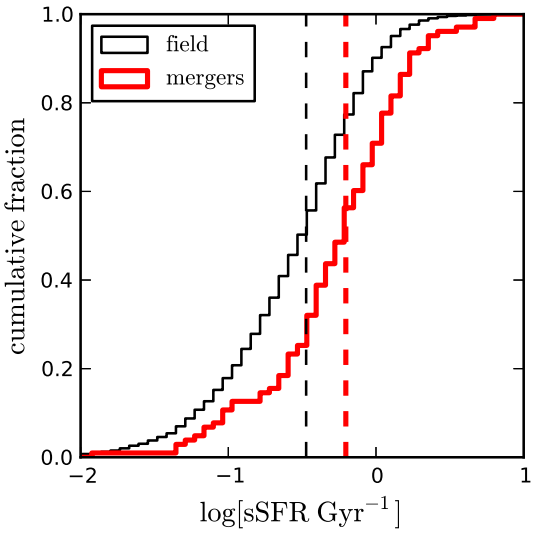

Figure 13. The cumulative distribution of sSFR for late-stage mergers and non-interacting galaxies from the zCOSMOS sample. The sSFR is derived from the *Spitzer*/MIPS 24μm flux. The median sSFR in late-stage mergers is a factor of 2.1 ± 0.6 larger than that in non-interacting galaxies.

enhanced by a factor of 2.1 ± 0.6 over the sSFR in the parent sample. This demonstrates that star formation in late-stage mergers proceeds at only a moderately higher rate than star formation in isolated galaxies. Using the slightly larger and deeper photo-z parent sample with the same stellar mass and redshift limits, we find a similar enhancement in the 24μm-derived sSFR in late-stage mergers.

As with the merger rate, the association of late-stage mergers with star forming galaxies may be affected by contamination from clumpy, star-forming galaxies, particularly at high redshift. Our peak-finding method may identify clumpy, star-forming galaxies as late-stage mergers, which would enhance the typical sSFR in late-stage mergers. However, we show in §4.1 that the contamination from non-merging, but clumpy, galaxies in $\sim 10\%$. Furthermore, the enhancement measured here is comparable or less than that measured using other merger selection methods, strengthening our claim that the contamination from star forming, isolated galaxies is small.

Kampczyk et al. (2013) draw similar conclusions about the [O II] λ3727-derived sSFR in kinematically-selected close pairs (see their Figure 13). They find the sSFR in pairs with separations smaller than $30\,h_{100}^{-1}$ kpc is enhanced by factors of $2-4$ compared to a stellar mass- and redshift-matched control sample. Using the [O II] λ3727 emission line as a SFR indicator (Moustakas et al. 2006; Maier et al. 2009), we also find an enhancement of 2.0 ± 0.5 in the median sSFR in late-stage mergers. The agreement between the 24μm- and [O II]-derived sSFRs suggests that the extinction in late-stage mergers is not significantly different from that in field galaxies. However the mean sSFR computed using [O II] emission is a factor of ~ 4 lower than the 24μm-derived sSFR.

We can add our sample of late-stage mergers to the more widely separated pairs in Kampczyk et al. (2013) to obtain the fraction of star formation between $0.25 < z < 1.05$ due to merging galaxies separated by less than $30\,h_{100}^{-1}$ kpc. Kampczyk et al. (2013) report that $6 \pm 1\%$

of galaxies are in kinematic pairs with projected separations less $30\,h_{100}^{-1}$ kpc. The sSFR in these galaxies is enhanced by a factor of 1.9 ± 0.6. In the same sample, we find $3.3\pm0.3\%$ of galaxies are late-stage mergers, which have sSFRs 2.1 ± 0.6 times above the median sSFR in the whole sample. Therefore, $18\pm5\%$ of star formation is associated with mergers, but only $8\pm5\%$ of all star formation can be considered "excess" star formation *triggered* by mergers. This modest enhancement in the star formation due to major mergers is in agreement with other studies of visually classified mergers and close pairs (Robaina et al. 2009; Jogee et al. 2009). In addition, these results also agree with semi-analytic models (Somerville et al. 2008), which report that only 7% of star formation is directly associated with major mergers.

Since the enhancement in sSFR for late-stage mergers is small, it is important to note that these systems are not starburst galaxies. The small shift in the SFR for late-stage mergers is in agreement analysis by Sargent et al. (2012). They suggest that the sSFRs for starburst galaxies and main sequence star-forming galaxies form a double Gaussian, in which the means are offset by only a factor of ~ 4. This is in contrast to other definitions of starburst galaxies, requiring SFRs an order of magnitude larger than predicted by the star-forming main sequence. While the majority of starburst galaxies are major mergers (e.g., Sanders & Mirabel 1996; Kartaltepe et al. 2010; Wu et al. 1998; Cui et al. 2001), the majority of late-stage mergers in our study are not starburst galaxies.

5.2. *AGN fraction*

In addition to triggering star formation, major mergers may drive black hole growth through AGN activity. Mergers can induce disk instabilities in coalescing galaxies that drive gas to the center of galaxies. This gas is used up both in star formation and in growing the black hole (e.g., Mihos & Hernquist 1996). Many simulations show that the periods of most intense star formation and black hole growth occur in late-stage mergers near coalescence (Mihos & Hernquist 1996; Springel et al. 2005; Di Matteo et al. 2007; Johansson et al. 2009). While simulations suggest that luminous accretion (i.e. QSOs) is dominated by major mergers, more than half of low-luminosity ($\log L_{\rm bol.}/L_{\odot} \lesssim 11$) AGN activity can be fueled by stochastic, non-major merger processes (e.g., Hopkins & Hernquist 2006; Hopkins et al. 2013). This is in agreement with studies of AGN host galaxies that demonstrate most AGN activity occurs in galaxies with undisturbed (non-merging) morphologies (e.g., Cisternas et al. 2011; Kauffmann et al. 2004; Liu et al. 2012; Kocevski et al. 2012). Nonetheless, there are many observations that show some enhancement in nuclear activity in galaxy pairs (Alonso et al. 2007; Silverman et al. 2011; Ellison et al. 2011; Koss et al. 2012; Ellison et al. 2013; Woods & Geller 2007, but see Darg et al. 2010a; Li et al. 2008; Barton et al. 2000). Using spectroscopic pairs out to $z\sim1$, Silverman et al. (2011) show the fraction of X-ray selected AGN with $10^{42}<L_{0.5-10\rm keV}<10^{44}$ erg s^{-1} increases from $3.8^{+0.3}_{-0.4}\%$ for isolated galaxies to $9.7^{+2.3}_{-1.7}\%$ for galaxies in pairs with a maximum projected separation of 75 kpc and a line-of-sight velocity separation less than 500 km s^{-1} . Despite this enhancement, only $\sim 25\%$ of AGN activity occurs in galaxy pairs, and an even smaller fraction, $\sim 18\%$ of AGN activity is *triggered* by close interactions.

We can improve the estimate of the fraction of AGNs due to merging by including late-stage mergers with the kinematic galaxy pairs in Silverman et al. (2011). In order to simplify the comparison, we use a parent sample identical to that of Silverman et al. (2011), and described above ($\log M_*/{\rm M}_{\odot}>10.4$ and $0.25\le z<1.05$). We select AGN based on their X-ray flux as measured by *Chandra* (Elvis et al. 2009). Due to the limited area of the *Chandra* survey, the zCOSMOS parent sample used here only contains 3474 galaxies of which 92 are late-stage mergers. The X-ray sources are matched to optical/IR sources as described in Civano et al. (2012). As in Silverman et al. (2011), we only consider X-ray sources with total fluxes ($0.5-10$ keV) greater than 1×10^{-15} erg cm^{-2} s^{-1} and luminosities larger than 2×10^{42} erg s^{-1}. The latter requirement eliminates galaxies in which the contribution from star formation to the X-ray flux is not negligible. Ninety-five percent of the X-ray sources have luminosities $L_{0.5-10\rm keV}<10^{44}$ erg s^{-1}. This ensures that most of the AGN hosts we examine are not AGN-dominated in the optical/NIR, and that the derived properties, especially stellar masses are reliable (Bongiorno et al. 2012; Salvato et al. 2011). The final sample contains 164 *Chandra* X-ray sources, which are certain to be AGN-dominated. Figure 14 shows the 6 late-stage mergers which are also X-ray selected AGN.

The left panel of Figure 15 shows the AGN fraction as a function of pair separation for our sample of late-stage mergers(filled square) and for more widely separated kinematic pairs (Silverman et al. 2011) drawn from the same parent sample. We define the AGN fraction as the fraction of late-stage mergers (close pairs) with an associated X-ray source. We compute the AGN fraction as in Silverman et al. (2011), equation 1. This formula down-weights compulsory zCOSMOS targets, which are X-ray selected, and likely to be AGN (Lilly et al. 2007). It also accounts for the spatially varying *Chandra* sensitivity by weighting each AGN by the fraction of galaxies in which the measured X-ray flux is below the sensitivity, i.e., the fraction of galaxies which *could* host each AGN. The values for the kinematic pairs in the left panel of Figure 15 are taken from the Bayesian likelihood analysis in Silverman et al. (2011). This method takes into account contamination of the control sample with galaxies in kinematic pairs in which only one member is observed spectroscopically. Since late-stage mergers fall into a single slit, this more sophisticated approach for calculating the AGN fraction is unnecessary. We find 6 late-stage mergers that are also X-ray selected AGN. Although the statistics are poor, the AGN fraction among late-stage mergers is $6.4\pm2.5\%$. This is marginally consistent with the AGN fraction in the field, $3.8^{+0.3}_{-0.4}\%$ (Silverman et al. 2011). At 95% confidence, we find that the AGN fraction in late-stage mergers is enhanced by less than a factor of 3.0, with a mean value of 1.7 ± 0.7, in agreement with (although less stringent than) Cisternas et al. (2011).

Given the upper limit on the enhancement of AGN activity associated with late-stage mergers, we can compute an upper limit for the AGN activity triggered by mergers. Following the same procedure as §5.1, the late-

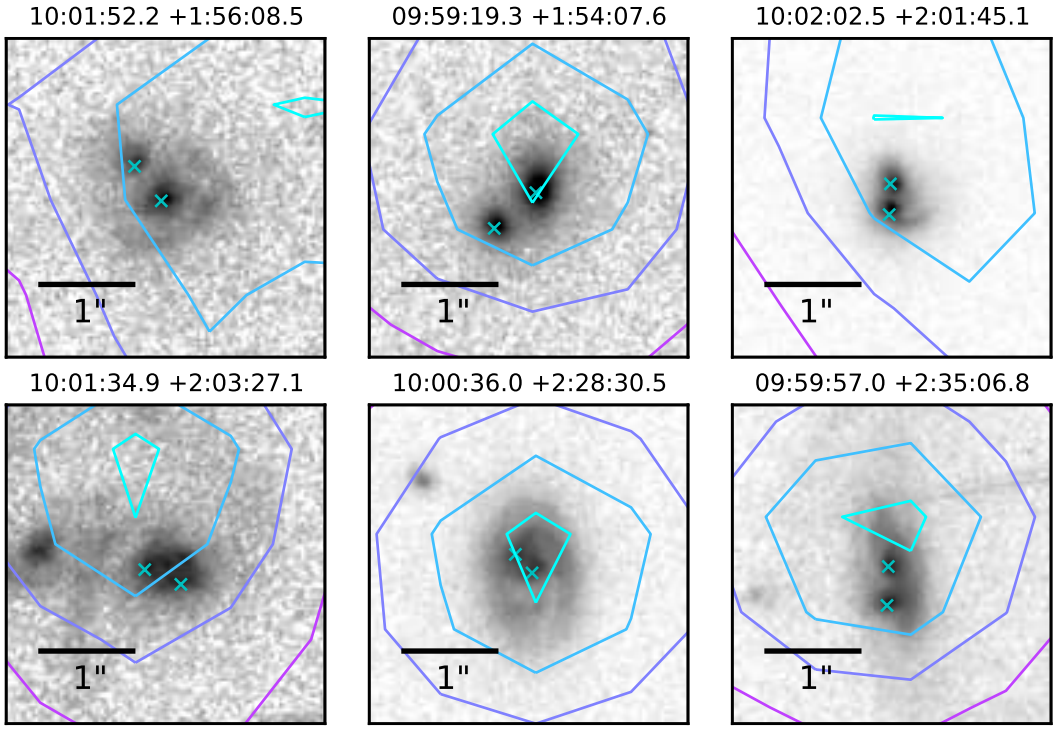

Figure 14. Images of the six late-stage mergers that are also X-ray selected AGN. The (blue) contours show the total $(0.5-7.0$ keV) flux from *Chandra* (Elvis et al. 2009). The (cyan) crosses show the position of the two peaks found by our merger-finding method. The galaxy in the lower middle panel may be a spiral galaxy.

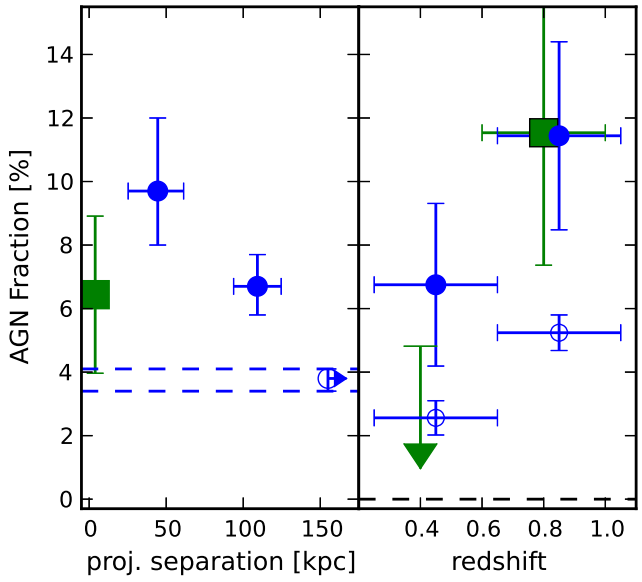

Figure 15. *Left:* The fraction of AGN in galaxy pairs at various projected separations. The 3 right points are from Silverman et al. (2011) (see their Figure 5). The empty symbol is the field value, corrected for unidentified kinematic pairs. The square shows the AGN fraction in late-stage mergers (6 mergers). The points are plotted at the median separation in each bin, and the horizontal error bars denote the interquartile range (25%−75%) of the galaxies in each bin. *Right:* The AGN fraction in pairs in two redshift bins. The squares denote late-stage mergers. There are no late-stage mergers in the low redshift bin and the error bar denotes the 1σ upper limit. The filled and empty circles are the AGN fraction in pairs separated by $<$ 75kpc, and the field, respectively, and are taken from Silverman et al. (2011). Note that in this panel, the field AGN fractions are not corrected for contamination by kinematic pairs and should be $\sim 0.5-1\%$ lower.

stage merger fraction in this sample is $3.0\pm0.3\%$ and the enhancement in the AGN fraction is at most a factor of 3 above the control sample. Therefore, the fraction of AGN activity associated with late stage-mergers is $< 9.0\pm0.9\%$ and the fraction of AGN activity *triggered* by late-stage mergers is at most $6.0\pm0.9\%$. Using the measured mean value for the AGN enhancement (1.7 ± 0.7), the fraction of AGN activity triggered by late-stage mergers is $2\pm2\%$. While Silverman et al. (2011) find approximately 1/4 of AGN are associated with kinematic pairs closer than 143 kpc, only $17.8^{+8.4}_{-7.4}\%$ of AGN can be directly contributed to the pair interaction. Combining the kinematic pairs with our late-stage mergers gives a total fraction of AGN activity triggered by mergers of $\sim 20\pm8\%$. As expected, including late-stage mergers does not significantly increase the fraction of AGN activity contributed to major mergers.

The right panel in Figure 15 shows the AGN fraction in pairs divided into two redshift bins, $0.25 \geq z < 0.65$ and $0.65 \geq z < 1.05$. Among late-stage mergers, all 6 X-ray selected AGN occur above $z = 0.65$. This boosts the AGN fraction at high redshift to $11.5\pm4.2\%$, which is statistically above the value for the field, and comparable to the boost seen for kinematic pairs separated by less than 75 kpc (Silverman et al. 2011). Note that in the right panel of Figure 15, the field AGN fraction is not corrected for contamination from kinematic pairs in which only one galaxy is observed. Since kinematic pairs do show an enhanced AGN fraction, correcting for this contamination will likely lower the field AGN fraction by $\sim 0.5-1\%$. Below $z \sim 0.65$, none of our late-stage mergers are also X-ray AGN. The error bar in Figure 15 shows the 1σ upper limit for the AGN fraction, which is consis-

tent with the AGN fraction in the field, albeit with large uncertainty. Although our results rule out a decrease in the merger rate at close separations, and suggest some enhancement in the AGN fraction at $z \gtrsim 0.7$, a larger sample is required to determine if any enhancement in the AGN rate for late-stage mergers is statistically significant.

From the X-ray and optical images alone, it is unclear if any of the late-stage mergers with AGN are dual AGNs. The possible dual AGN, CID-42 (Comerford et al. 2009; Civano et al. 2010), is excluded from the sample above since the measured stellar mass of the system is below $2.5 \times 10^{10} M_{\odot}$, however our method does select CID-42 as a late-stage merger. We have examined the spectra for the 6 mergers with AGN and find no evidence for velocity offsets, suggesting that only one of the black holes in the system is actively accreting. Nonetheless, since the late-stage mergers are selected to have two, concentrated central cores, this sample would be well-suited to searches for galaxies with dual AGN.

5.2.1. *AGN in the photo-z sample*

We can check the fraction of mergers with AGN using the photo-z sample. For the photo-z sample, we use the same stellar mass and redshift cuts as the spectroscopic sample. However, we exclude X-ray sources that are best-fit by a Type I AGN/QSO template (Salvato et al. 2011).Since we identify late-stage mergers based on the flux ratio of two central peaks, our method is poorly-suited to selecting companions of bright Type I AGN, in which the optical flux is dominated by a single point source. This means that the AGN fraction reported here is for lower luminosity, obscured AGN, not bright Type I AGN.

Using the photo-z sample, we find 8 late-stage mergers that are *Chandra*-detected X-ray AGN with $L_{[0.5-10\ \mathrm{keV}]} > 2 \times 10^{42}$ erg s^{-1}, 4 of which are also identified in the spectroscopic sample. The missing 2 galaxies are excluded because of differences in the masking in the $K-$band and $I-$band selected catalogs, used for the photo-z and spec-z samples (see Ilbert et al. 2013; Lilly et al. 2007). These 8 late-stage mergers yield an AGN fraction of $5 \pm 2\%$, consistent with the AGN fraction fraction found above and that in the field. Because of the high degree of overlap between the photo-z and spec-z galaxy samples, all our results on the AGN fraction are highly correlated and do not add significant statistical power. Complete coverage of the COSMOS area with *Chandra* will improve the statistics of these results by a factor ~ 2 and yield a larger sample of AGN associated with mergers (Civano et al., *in prep*).

As with the star formation rates, we find that, although AGN activity may be slightly enhanced in late-stage mergers, mergers do not drive the majority of AGN activity, and, hence, black hole growth. Including late-stage mergers along with more widely separated pairs, only $\sim 20\%$ of AGN activity is triggered by mergers, and late-stage mergers are responsible for at most 6% of AGN activity. The small increase in AGN activity associated with close pairs is in agreement with previous studies (Ellison et al. 2013; Alonso et al. 2007) and suggests minor mergers or secular processes within galaxies drive the majority of low-luminosity AGN activity. Similarly, while the star formation rate in late-stage mergers is typically enhanced compared to a control sample, the enhancement is less than a factor of 2 and only $8 \pm 5\%$ of star formation can be contributed to kinematic pairs or late-stage mergers. The similarity between the AGN enhancement and SFR enhancement in merging galaxies (see also Silverman et al. 2011) suggests that star formation and AGN activity are physically coupled, as is expected from simulations of gas-rich major mergers (Mihos & Hernquist 1996; Barnes & Hernquist 1992; Hernquist 1989; Hopkins et al. 2006, 2008).

It is possible that our focus on late-stage mergers ignores other phases of galaxy merging with larger enhancements in AGN activity and star formation (see Scudder et al. 2012). The bright QSO phase may occur when the two nuclei are closer to coalescence (e.g. Di Matteo et al. 2005; Hopkins et al. 2008). However, by combining kinematic pairs with late-stage mergers, we can observe galaxy mergers from separations of $100\, h_{100}^{-1}$ kpc until shortly before coalescence. Furthermore, the $0.5 - 8$ keV X-ray selection for AGN may exclude highly obscured AGN, which would be visible in the infrared (e.g., Satyapal et al. 2014) or harder X-ray bands (e.g., Koss et al. 2011). Using WISE-selected AGN in SDSS, Satyapal et al. (2014) find an enhancement of the AGN fraction in nearby post-merger galaxies of a factor $10 - 20$, suggesting the AGN in late-stage mergers are highly obscured. Nonetheless, the low enhancement in X-ray selected AGN and star formation activity in late-stage mergers and kinematic pairs reconfirms the results that galaxy and black hole growth are not solely driven by major mergers.

6. SUMMARY

Although mergers of dark matter halos underpin theories of structure and galaxy formation, the actual role of galaxy mergers is less clear. In this work, we seek to expand the study of merging galaxies to galaxy pairs with small separations. By including late-stage mergers with samples of more widely separated (as yet not merging) pairs, we can obtain a better understanding of the role of mergers in galaxy evolution since $z \approx 1$. To that end, we develop a method to identify late-stage galaxy mergers using *HST* images.

We utilize a high-pass filter which easily detects the bright, concentrated, central cores of both member galaxies of a merger before coalescence. By implementing limits on the flux ratio and brightness of the measured peaks, we are able to produce a clean sample of 2055 galaxy mergers from COSMOS ACS $I-$band images of galaxies brighter than $I = 23$. These late-stage mergers have two intact galaxy nuclei that are separated by less than 8 kpc. If we restrict the parent sample to a mass-complete ($\log M_*/M_{\odot} > 10.6$) sample of galaxies in the redshift range $0.25 < z < 1.0$, with pair separations between 2.2 and 8 kpc, we find 136 late-stage mergers, which represents $2.3 \pm 0.2\%$ of the massive galaxy population, or $4.8 \pm 0.5\%$ when corrected for contamination and incompleteness. The sample of late-stage mergers identified here is distinct from other samples of merging galaxies, such as kinematic pairs, and morphologically disrupted galaxies identified by CAS or Gini/M20.

We create mock images of mergers by placing two real galaxies in one postage stamp and use these to test the completeness and contamination in our sample. Al-

though the sample suffers little from contamination (10% from clumpy, non-merging galaxies and 20% from minor mergers), we only successfully select $\sim$ 20% of all major mergers, and the selection efficiency decreases with increasing redshift. Our method is most successful for mergers between concentrated early-type galaxies, selecting 80% of all simulated mergers, independent of redshift.

Using the sample of late-stage mergers we study both the evolution of the merger rate and the properties of merging galaxies. Our results can be summarized as follows:

- For galaxies with stellar masses above $\log M/\mathrm{M}_\odot > 10.6$, we find that the fraction of mergers evolves as $f_{\mathrm{merge}} \propto (1+z)^{3.8\pm0.9}$ when corrected for incompleteness, and contamination from minor mergers, non-mergers and line-of-sight superpositions. Despite uncertainties in the sample completeness, and the merger timescale, T_{obs}, the normalization of the fractional merger rate, $\Re_{\mathrm{merge}}$, agrees well with that found in previous studies. The measured evolution in the merger rate becomes significantly flatter if we remove the redshift-dependent correction for incompleteness of the sample, $\Re_{\mathrm{merge}} \propto (1+z)^{0.8\pm0.8}$.

- Dividing the sample into quiescent, star-forming, low mass, and high mass galaxies, we find that the merger rate for star-forming galaxies is a strong function of redshift, $\Re_{\mathrm{merge}} \propto (1+z)^{4.5\pm1.3}$, while that for quiescent galaxies is a mild function of redshift, consistent with no evolution, $(1+z)^{1.1\pm1.2}$. Therefore, among massive galaxies, the increase in the total merger rate is driven by the increase in the merger rate for star-forming galaxies and by the increasing fraction of massive star-forming galaxies at high redshift. Lower mass ($10.6 < \log M/\mathrm{M}_\odot < 10.9$) galaxies also exhibit a steeper merger rate evolution than higher mass ($\log M/\mathrm{M}_\odot > 10.9$) galaxies: $(1+z)^{5.1\pm1.3}$ compared to $(1+z)^{2.7\pm1.1}$. These results use different corrections for completeness for star-forming (late-type) mergers and quiescent (early-type) mergers. Although the merger rate slopes are not as steep without the corrections for incompleteness, the merger rate for star-forming (low-mass) galaxies still evolves more than that of quiescent (high-mass) galaxies. This shows that the differences in the merger rates as a function of stellar mass and SFR are robust. Furthermore, these differences suggest that measurements of the merger rate as a function of redshift are very sensitive to the sample of galaxies.

- Examining the properties of late-stage mergers, we find that the SFR in late-stage mergers with $\log M_*/\mathrm{M}_\odot > 10.4$ is enhanced by a factor of 2.1 ± 0.6 compared to non-interacting galaxies. This is similar to the enhancement found for kinematic galaxy pairs using the same parent sample (Kampczyk et al. 2013). Only $18 \pm 5\%$ of star formation between $z = 0.25$ and $z = 1.05$ is associated with late-stage mergers or pairs separated by less than $30\,h_{100}^{-1}$ kpc. However, the excess star formation that can be attributed to major mergers is only half of that.

- The AGN fraction in late-stage mergers at $z > 0.5$ is enhanced by a factor of 2.2 ± 0.8 compared to the field. For the entire redshift range, $0.25 < z < 1.05$, we do not measure a statistically significant enhancement in AGN activity. At most, the AGN activity in late-stage mergers between $0.25 < z < 1.05$ is enhanced by a factor of 3 above the activity in field galaxies. Together with more widely separated pairs, $20 \pm 8\%$ of AGN activity is induced by mergers at separations less than 143 kpc. The fraction of AGN triggered by late-stage mergers and kinematic pairs is similar to the fraction of SFR activity triggered by the same class of mergers. This suggests that the processes responsible for star formation and AGN activity in major mergers are coupled, indicating a co-evolution scheme (Jahnke et al. 2009; Cisternas et al. 2011; Schramm & Silverman 2013).

The measurement of the blue galaxy merger rate is particularly sensitive to morphological k-corrections and the increasing fraction of blue, star-forming, clumpy galaxies at high redshift. Because galaxies appear clumpier at blue rest frame wavelengths and the entire galaxy population contains more clumpy, star-forming galaxies at high redshift, we expect our peak-finding method to detect more late-stage merger candidates at high redshift. We plan to address this by applying our peak-finding method near-infrared data WFC3 *HST* data from the CANDELS survey (Koekemoer et al. 2011; Grogin et al. 2011). Performing this study at longer wavelengths may also help increase the completeness of our merger sample. Galaxies appear more bulge-dominated and concentrated at longer wavelengths and our merger-finding method is significantly more sensitive to mergers between concentrated, early-type galaxies than mergers between late-type galaxies.

Although we have examined the SFRs and X-ray emission of late-stage mergers, resolved properties of the mergers require additional data. For instance, we have a sample of $\sim$ 20 late-stage mergers with significant X-ray detections and 2 concentrated central cores. Although the X-ray detection cannot resolve the merging galaxies, these sources provide an excellent parent sample for spectroscopic searches for dual AGN (e.g., Comerford et al. 2009; Liu et al. 2010; Civano et al. 2010). By focusing only on X-ray AGN, we are only studying a subset of AGN. There are many AGN selected in *IRAC* (Donley et al. 2012), radio (Smolčić et al. 2008), and optical/infrared (Fiore et al. 2008; Dey et al. 2008). Increasing the sample size of AGN will increase the number of AGN in late-stage mergers. Further work is needed to determine if the *fraction* of AGN activity associated with late-stage mergers will also increase using AGN selected in the optical, infrared, or radio.

Obtaining a sample of late-stage mergers between $1 \lesssim z \lesssim 2$ would allow us to continue to measure the evolution of the merger rate at higher redshifts. Recent spectroscopic studies suggest that the merger rate increases quickly beyond $z \sim 1$ (e.g., López-Sanjuan et al. 2013; Tasca et al. 2014). Expanding the sample to higher redshift requires high resolution and signal-to-noise data in the near infrared. Switching to the longer wavelengths eliminates the effects of morphological $k-$corrections, as

there is evidence that galaxies typically have more structure at shorter wavelengths (e.g., Kuchinski et al. 2000). Near-infrared WFC3 *HST* data from the CANDELS survey (Grogin et al. 2011; Koekemoer et al. 2011) could be used for such a study. Additionally, since the star formation and AGN activity also continue to grow with redshift, expanding the sample of mergers to higher redshift will increase the statistical significance of the sample of late-stage mergers with ongoing star formation and AGN activity. This will help determine the role of major mergers in the growth of galaxies and super-massive black holes at their peak epoch of formation.

We thank the referee for their insightful comments which greatly improved this work. We also thank Richard Massey and Kevin Bundy for helpful comments on a draft. This work was supported by World Premier International Research Center Initiative (WPI Initiative), MEXT, Japan. ST acknowledges support from the Lundbeck Foundation. The Dark Cosmology Centre is funded by the Danish National Research Foundation. This research has made use of the NASA/IPAC Infrared Science Archive, which is operated by the Jet Propulsion Laboratory, California Institute of Technology, under contract with the National Aeronautics and Space Administration. This research made use of APLpy, an open-source plotting package for Python hosted at http://aplpy.github.com

APPENDIX

APPENDIX A: SIMULATED MERGER IMAGES

In order to test our merger-finding algorithms, we create a sample of mock mergers by coadding real galaxy images from our original sample to create new postage stamps. These fake merger images have the same properties as the real galaxy images and allow us to test both the completeness and contamination of our merger selection. In particular, the mock mergers will have the same redshifts, magnitudes, morphologies, and merger ratios as the real galaxy population. Because the fraction of real mergers is small, they represent a small contamination in our sample of mock mergers. While these simulations are realistic in many ways, they do not include any structural changes wrought by the merger in the images. However, since our method is sensitive to only the brightest features in merging galaxies, this omission is likely unimportant. Below, we focus on mergers in which the total mass is larger than $4 \times 10^{10} M_{\odot}$ and the redshift is between $0.25 < z < 1.0$. These are the cuts in §4 and ensure the sample is complete at all redshifts.

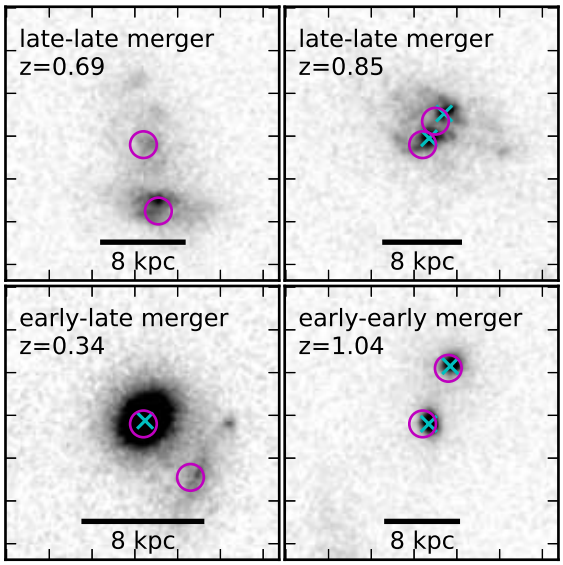

Figure 16. Example mock merger images. The circles show the position of the coadded galaxies, while the crosses show the positions of the detected peaks. Both galaxy mergers on the right are sucessfully detected and pass the cuts implemented to remove contaminants. For the merger in the upper left, both galaxies are late-type and too diffuse to be detected. For the merger in the lower left, the flux ratio between the two galaxies is too large to be detected.

To create a mock merger postage stamps, we randomly select 2400 galaxies from our photo-z sample. For each selected galaxy, we select at random a second galaxy at approximately the same photometric redshift ($\Delta z < 0.02$) as the first selected galaxy. This ignores any contamination from chance superpositions at widely different redshifts, which we address statistically in §4.1. We then coadd the *HST*/ACS postage stamp images of these galaxies. For each galaxy pair, we make 8 postage stamps with different separations between the galaxy centers, spanning from 0.1 to 10 kpc. Using the ZEST morphology parameter (Scarlata et al. 2007), we create 3 additional samples of 1200 mock mergers with specific morphologies: a sample of mergers between two early-type galaxies (ZEST=1), a sample between late-type galaxies (ZEST=2), and a mixed sample (ZEST=1 and 2). We apply the median ring filter to all these mock images and examine the results. Figure 16 shows four example mock merger images. The circles denote the two galaxies which have been super-imposed. Because of the coaddition, these mock images are a factor of $\sqrt{2}$

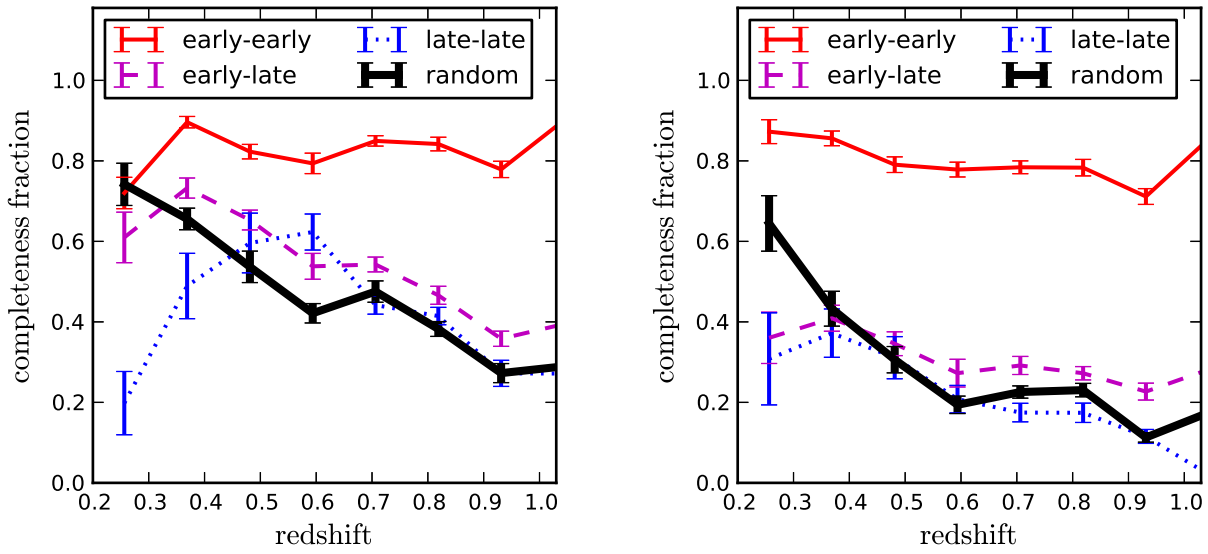

Figure 17. The completeness of the late-stage major mergers in simulated images as a function of redshift, before applying cuts in flux ratio for contamination (left) and after applying cuts (right). The thick black line shows the completeness for a random sample of galaxies, with a representative morphological mix. While the other lines show the completeness for mock mergers in which the merging galaxies are both early types (red, solid), both late types (blue, dotted), and mixed (magenta, dashed). The morphologies are determined by the ZEST parameter. The error are derived by bootstrap resampling. The completeness is a stronger function of morphology than redshift.

nosier than the original images. However, because we are creating merger images by coadding images from our sample, the mock mergers are up to a factor of 2 brighter than the real galaxies in the sample. These effects approximately cancel out and we neglect the differences in signal-to-noise between the mock mergers and the real galaxy images.

Figure 16 also demonstrates that our method does not detect all mock mergers (blue ×s in Figure 16). Our selection is particularly incomplete for mergers among late-type galaxies, in which neither galaxy has a dominant bulge. The left panel of Figure 17 indicates our completeness as a function of redshift (black solid line). In this figure, we examine the completeness for major mergers ($> 1:4$) with separations between 2.2 and 8.0 kpc, without applying any cuts in flux ratio, while the right panel includes cuts in flux ratio (see below). Beyond $z \sim 0.5$, our method only detects 20% of the mock late-stage mergers. Dividing the sample by the ZEST morphology of the merging galaxies shows that the completeness is a strong function of morphology. The median ring filter selects 80% of early-type mergers, but only $\sim 40\%$ of late-type mergers. This is expected, since our method requires a strong central bulge in order to detect a peak. However, in comparing the merger rates of early and late type galaxies, it is important to note their very different completeness fractions. Furthermore, the decrease in the completeness up to $z \sim 0.5$, suggests that our merger rate evolution may be underestimated, as we are missing $\sim 2\times$ as many galaxies at high redshift than at low redshift.

Figure 18 shows the completeness as a function of pair separation, similarly divided by galaxy morphology. For all morphologies, the completeness is independent of pair separation beyond $\sim 2-3$ kpc. This is driven by the size of the median ring filter (2.2 kpc at $z = 1$). The lower panel shows the fractional error in our measurement of the pair separation. For large separations, the separation is well-measured. However, for small real separations, the measured separation is typically too large. By cutting off the pair separations at 2.2 kpc, we introduce some contamination from smaller separation pairs, particularly at lower redshifts. Determining the exact fraction of this contamination would require knowledge of the spectrum of real pair separations, which we have not included in these simulations. However, we can assume that the number of mergers at small separations will be smaller than those at large separations, so we expect this contamination to be small. In particular, the contamination from other galaxy structures and minor mergers is likely to be much larger, and can be measured using our simulated merger images.

Because our mock merger images use real galaxies, we can ascertain how often galactic sub-structures, such as bars, spiral arms, and star-forming clumps, are selected by the median ring filter. These features are typically fainter than galaxies, and by implementing a cut on the ratio of the peak flux to the total galaxy flux, we can eliminate a substantial fraction of the contamination for galaxy substructure. Figure 19 shows the distribution of peak fluxes for peaks associated with merging galaxies and peaks associated with galaxy substructure. The substructure peaks are typically fainter. In order to eliminate these detections, we require that the detected peaks contain at least 3% of the total galaxy flux. This reduces the contamination by extraneous peaks to $\sim 10\%$, while keeping the completeness of *detected* peaks at $\sim 80\%$. Lowering this threshold to 0.5% does not significantly affect our results. Before applying our method to different imaging data, similar simulations should be conducted in order to determine the threshold value.

In addition to contamination from star-forming clumps and galactic substructure, our merger finding method is somewhat sensitive to minor mergers. Since we are only interested in studying late-stage major mergers, it is important to understand the contamination from minor mergers. To create a mock merger sample with a realistic fraction of minor mergers, we build a sample of 2400 mock mergers in which one member of the pair is brighter than $I = 20.5$.

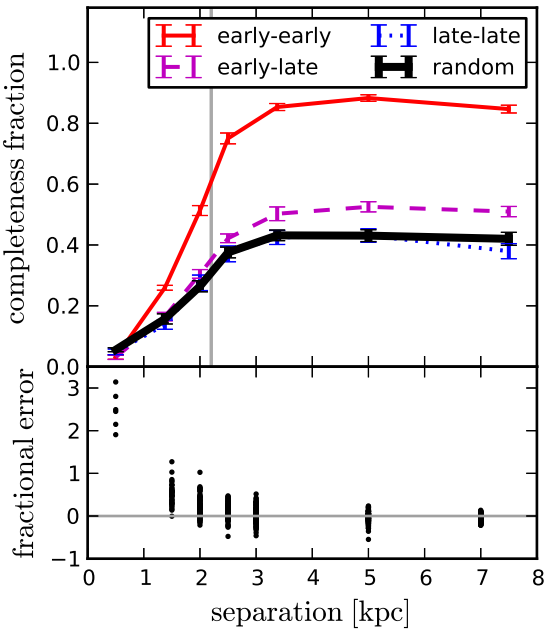

Figure 18. *Top*: The completeness of the mock mergers as a function of pair separation. Note that each galaxy pair was simulated at a discreet set of separations. The completeness drops sharply for separations comparable to the median ring filter size. The different lines show the completeness for different morphologies for the members of the merger, as in Figure 17. The vertical line shows the cut made in separation at 2.2 kpc. *Bottom:* The fractional error in the measured peak separation compared to the real separation for the 'random' sample of morphologies only. The separation is reasonably well measured beyond a few kpc. However, small separations are typically overestimated which will lead to contamination of our sample by mergers with separations < 2.2 kpc.

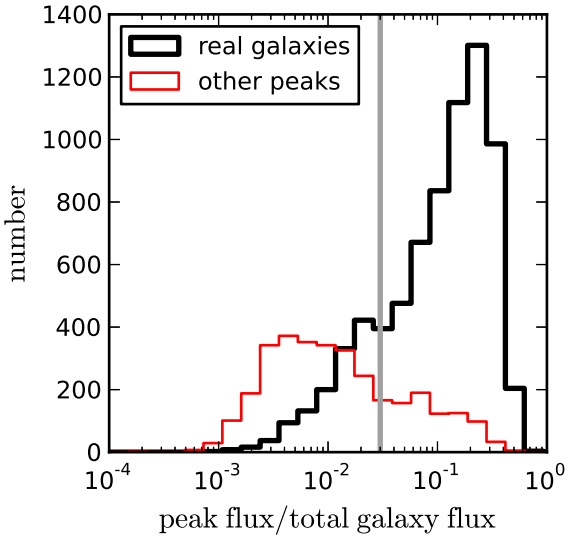

Figure 19. Distribution of the detected peak flux ratios. The thick line histogram shows the distribution of peak to total flux for detected galaxy sources in the mock merger images. The thin line shows the distribution of extraneous peaks detected. By putting a cutoff at 3%, the contamination from extraneous peaks is 10%.

This ensures that, from a sample of galaxies with $I < 23$, we include a realistic spectrum of merger ratios down to $1:10$. Note that our algorithm only measures the flux ratio of the merger, *not* the underlying mass ratio, which requires color information about the separate galaxies. However, in our mock merger images, we find that the *real* flux ratio of a merger is well-correlated with the mass ratio, and that the flux ratio of 0.25 corresponds approximately to a mass ratio of 0.25.

Figure 20 shows the contamination rates for our sample of detected mergers, including major and minor mergers, as well as false positives, i.e. mergers made of star forming clumps instead of the two galaxies inserted into the mock image. We exclude mergers with a observed flux ratio smaller than 0.25. Overall, 70% of the detected late-stage mergers are real major mergers, and only 10% of mergers are false positives, as expected from the peak flux to total flux cut explained above. The total fraction of minor mergers is 20%, and the contamination is worse at lower flux

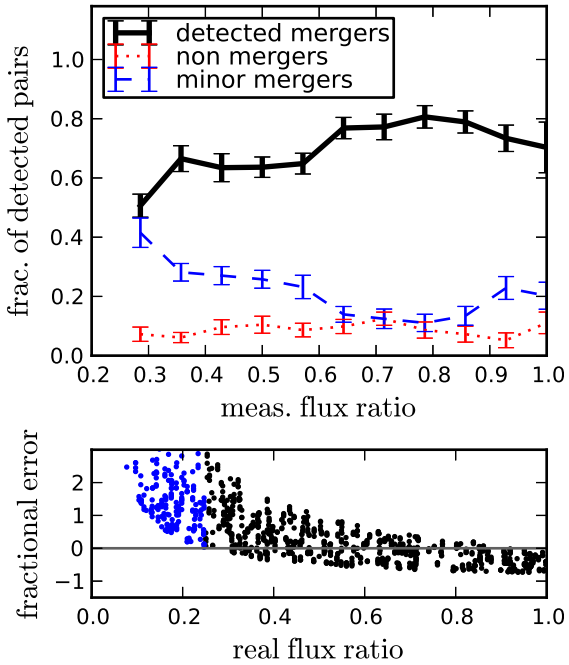

Figure 20. *Top:* The fraction of detected mergers which are major mergers (solid line), minor mergers (dashed line) and contaminants (dotted lines). The major (minor) mergers consist of two galaxies with a flux ratio larger (smaller) than 0.25. The contaminants are detected late-stage mergers which do not match the mock galaxies placed in each image. These include detections of galactic substructure. *Bottom:* The fractional error in the measured flux ratio as a function of real flux ratio. For small real flux ratios, our method typically overestimates small flux ratios, which leads to a contaimination from minor mergers.

ratios. The lower panel in Figure 20 shows the fractional error in the measured flux ratio. While the measured flux ratio correlates with the real flux ratio, the errors are extremely large, particularly at small real flux ratios. Better measurements of the flux ratio could be obtained by fitting a late-stage merger with two realistic galaxy profiles centered on each detected peak. However, in this work, we only use the measured flux ratio to discriminate between major and minor mergers. By only selecting mergers with a flux ratio larger than 0.25, we only eliminate 15% of the detected major mergers and 30% of minor mergers. Note, that the median ring filter is less sensitive to minor mergers than major mergers, and that many minor mergers are eliminated by the peak flux to total flux cut of 3%. Both of these effects further help to limit contamination from minor mergers.

Taken together, our cuts in peak to total flux ratio, and peak to peak flux ratio, do affect the overall completeness, particularly the late-type galaxy merger completeness. After implementing the flux ratio cuts, the overall completeness drops to $20-25\%$ (see the right panel of Figure 17), with most of the decrease coming from late-type mergers. However, these cuts are important since they significantly decrease the contamination from star forming clumps and minor mergers. Using the results of Figure 17 and 20, we can correct the measured late-stage merger fractions for incompleteness and contamination and use the corrected fractions to determine the merger rate evolution. In studying the internal properties of late-stage mergers, we cannot include a correction for incompleteness. However, in this case, it is more important to have a minimally contaminated sample of late-stage mergers, as significant contamination will mask any differences between the field population and the merger population.

APPENDIX B: COMPARISON TO CAS AND GINI-M_{20}

In order to better understand the poor overlap between our sample of late-stage mergers and mergers selected based on their Gini (G), M_{20} and asymmetry (A) values, we examine a small random set of galaxy images. A galaxy is considered a merger by the Gini-M_{20} method if $G > -0.12M_{20} + 0.38$ (Lotz et al. 2008a). A galaxy is considered a merger based on its asymmetry if $A > 0.35$ (Conselice 2003). The morphology measurements G, M_{20}, and asymmetry (A) values are taken from Cassata et al. (2005). Note that the deblending done by Cassata et al. (2005) leads to different values for the morphology metrics than those derived directly from the images shown here. However, because we are looking for merging, deblending close pairs may not always be desirable, and we include differences in the deblending as part of our comparison.

The Gini-M_{20} and asymmetry merger selections were designed to work in the rest frame $B-$band at low redshift (e.g. Conselice 2003; Lotz et al. 2008a). In order to compare the results to higher redshifts, morphological k-corrections need to be taken into account. By using galaxies at redshifts above $z \sim 0.6$, the observed $I-$band images are close to the rest frame $B-$band images and corrections to the measured G, M_{20}, and A can be neglected. We do include a correction of $\delta A = 0.05$ for the effect of surface brightness dimming at high redshift (see Conselice et al. 2009; Conselice 2003; Conselice et al. 2003).

Figure 21 shows late-stage mergers selected by our method that are not selected by the Gini-M_{20} criterion. Panels b, c, d, g, and h show galaxies with Gini and M_{20} values close to the division line. In panel a, the detected peaks are

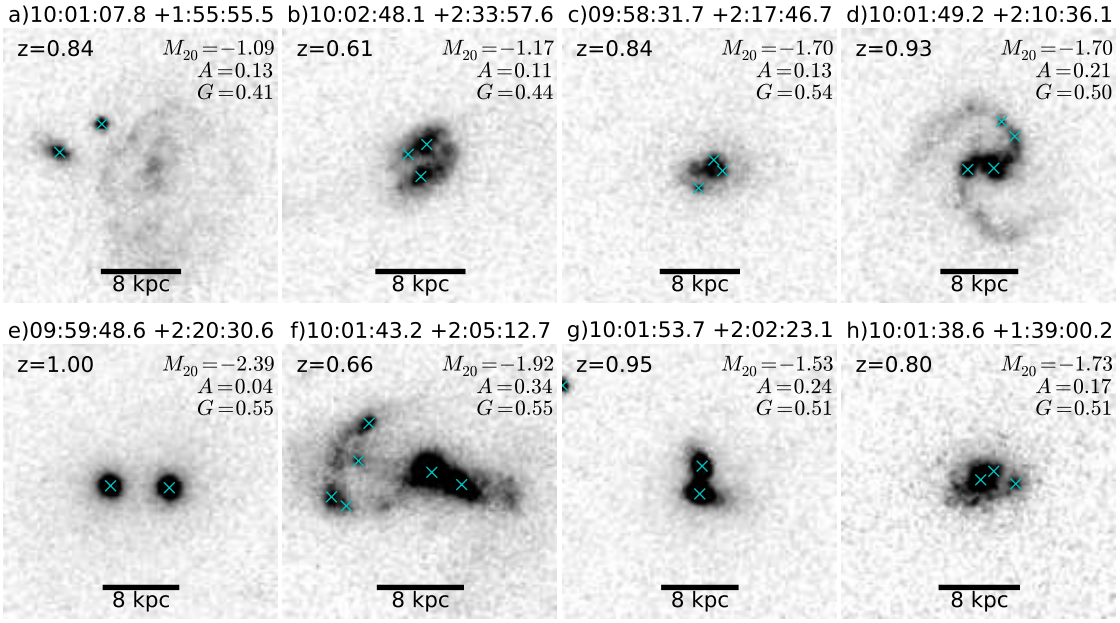

Figure 21. Examples of galaxies which are late-stage mergers but are *not* detected as mergers by the Gini-M_{20} method (Lotz et al. 2008a). We only examine galaxies with $z > 0.6$ in order to minimize the effects of morphological k-corrections to the rest frame $B-$band. Crosses show all detected peaks, before any cuts on projected separation or flux ratio. The images are shown with an arcsinh stretch and with the same scaling.

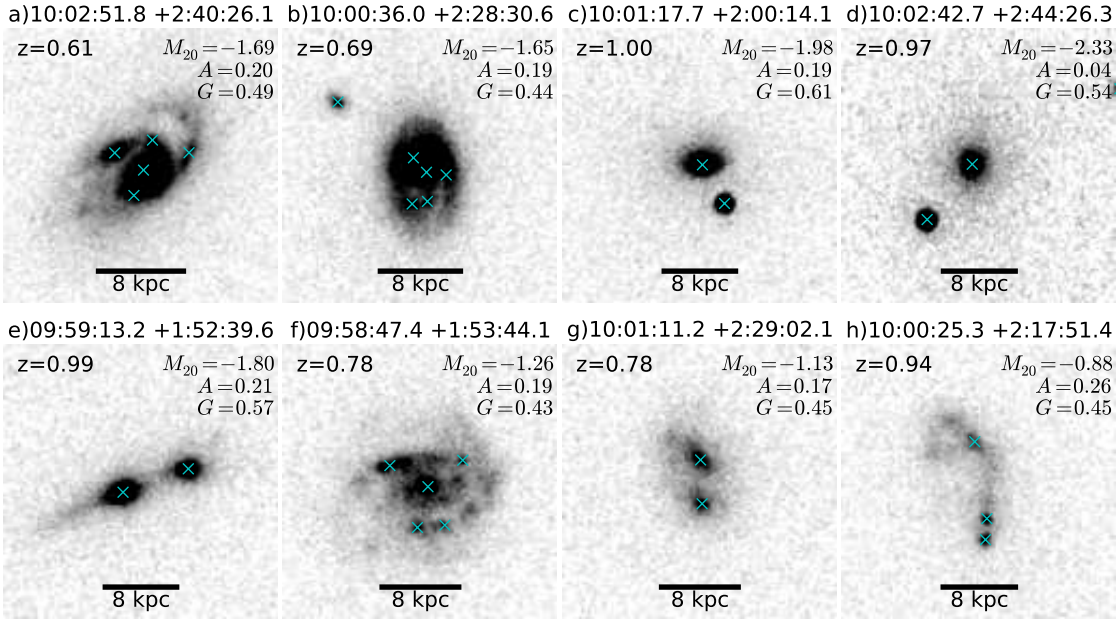

Figure 22. Examples of galaxies which are late-stage mergers but are *not* selected as mergers based on their asymmetry around a 180° rotation ($A > 0.35$, (see Conselice 2003)). We use the asymmetry measurements from Cassata et al. (2005) and include a correction of 0.05 for the surface brightness dimming (Conselice et al. 2009). We only use galaxies with $z > 0.6$, which limits the morphological k-corrections when comparing to the rest frame B-band. The images have the same stretch and scaling as those in Figure 21.

well-separated from the main galaxy and are likely a separate system. In panels e and f, the central peaks are well enough separated to be deblended before measuring the morphology. This will lower the M_{20} coefficient in particular. In general, the galaxies our merger method selects are highly concentrated, which leads to lower M_{20} values than for other mergers.

Figure 22 shows late-stage mergers with $A < 0.35$ that are not considered mergers based on their asymmetry. Galaxies in panels c, d, g, and h likely have low asymmetry values due to differences in deblending. However, it is worth noting that an equal mass merger between two similar galaxies will be symmetric about an 180° rotation, which may contribute to the low A values in the case of galaxies in panels d and g. As with the galaxies in Figure 21, the galaxies shown here are highly concentrated, which also tends to lower the asymmetry value.

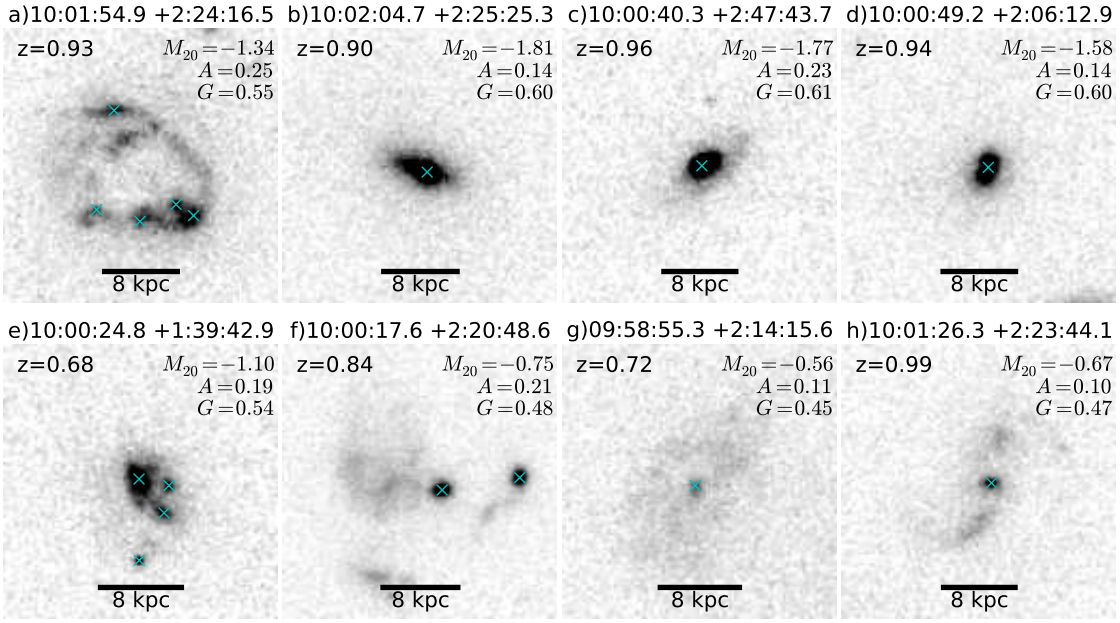

Figure 23. Examples of galaxies which are *not* late-stage mergers but are selected as mergers by the Gini-M_{20} method (Lotz et al. 2008a). The redshift range is the same as in Figure 21 The images have the same stretch and scaling as those in Figure 21. Most of these systems would be characterized as minor mergers, and therefore missed by our method.

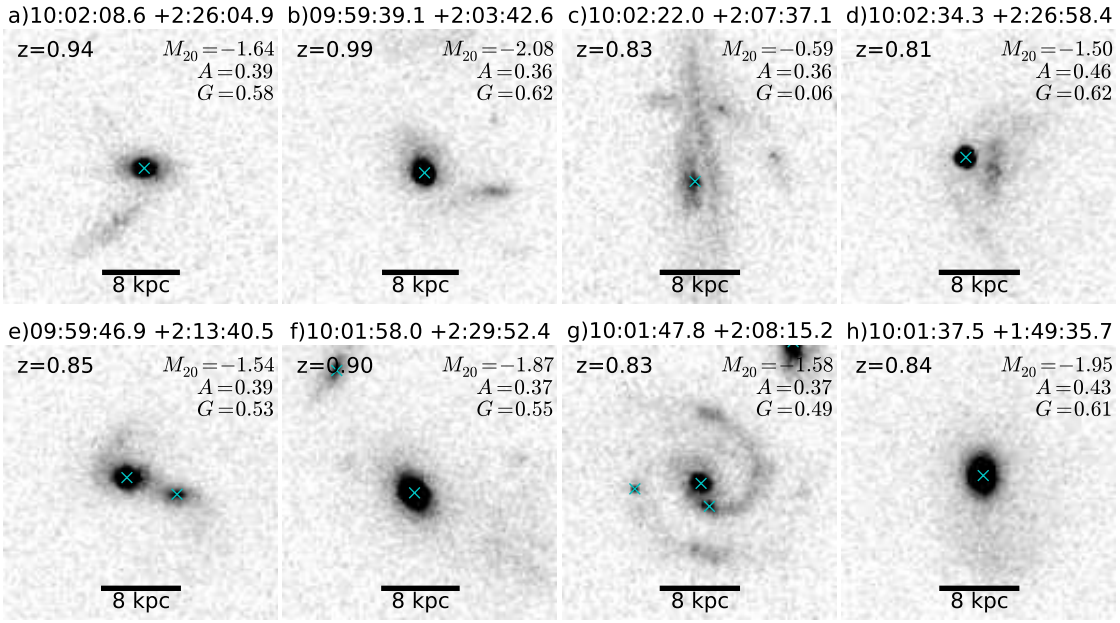

Figure 24. Examples of galaxies which are *not* late-stage mergers but are selected as mergers based on their asymmetry around a 180° rotation ($A > 0.35$ (see Conselice 2003)). The images have the same stretch and scaling as those in Figure 21.

Figure 23 shows instead the galaxies detected as mergers by the Gini-M_{20} criterion but not selected as late-stage mergers. Panels *b*, *c*, *d*, *g*, and *h* show galaxies with only one bright central peak. The galaxy in panel *d* may have two bright nuclei, but they are not separable by our method. The peaks detected in panels *a* and *e* are too faint compared to their host galaxy to be included by our method. Our method would characterize these galaxies as star-forming, not merging. The peaks detected in panel *f* are separated by slightly more than 8 kpc and are therefore excluded from our sample.

Figure 24 shows galaxies which are selected as mergers based on their asymmetry, but not by our median ring filter method. The asymmetric features in almost all of these galaxies are too faint to be detected by our method. The mergers in panels *e* and *g* both have flux ratios below our threshold of 0.25 and would be considered minor mergers. Indeed, many of the galaxies not detected by our method but detected by other methods are minor mergers, in which one component is significantly fainter than another, or the companion is no longer visible and only other tracers of

the merger remain. This suggests our merger finding method may be complementary to other merger finding methods better suited to finding minor mergers.

REFERENCES

Abraham, R. G., Valdes, F., Yee, H. K. C., & van den Bergh, S. 1994, ApJ, 432, 75
Abraham, R. G., van den Bergh, S., & Nair, P. 2003, ApJ, 588, 218
Alonso, M. S., Lambas, D. G., Tissera, P., & Coldwell, G. 2007, MNRAS, 375, 1017
Balogh, M. L., Morris, S. L., Yee, H. K. C., Carlberg, R. G., & Ellingson, E. 1999, ApJ, 527, 54
Barnes, J. E. & Hernquist, L. 1992, ARA&A, 30, 705
Barnes, J. E. & Hernquist, L. E. 1991, ApJ, 370, L65
Barton, E. J., Geller, M. J., & Kenyon, S. J. 2000, ApJ, 530, 660
Bell, E. F., Phleps, S., Somerville, R. S., Wolf, C., Borch, A., & Meisenheimer, K. 2006, ApJ, 652, 270
Berrier, J. C., Bullock, J. S., Barton, E. J., Guenther, H. D., Zentner, A. R., & Wechsler, R. H. 2006, ApJ, 652, 56
Bolzonella, M., et al. 2010, A&A, 524, A76
Bongiorno, A., et al. 2012, MNRAS, 427, 3103
Bordoloi, R., Lilly, S. J., & Amara, A. 2010, MNRAS, 406, 881
Bournaud, F., Elmegreen, B. G., & Elmegreen, D. M. 2007, ApJ, 670, 237
Bridge, C. R., Carlberg, R. G., & Sullivan, M. 2010, ApJ, 709, 1067
Brusa, M., et al. 2010, ApJ, 716, 348
Bundy, K., Fukugita, M., Ellis, R. S., Targett, T. A., Belli, S., & Kodama, T. 2009, ApJ, 697, 1369
Carlberg, R. G., Pritchet, C. J., & Infante, L. 1994, ApJ, 435, 540
Cassata, P., et al. 2005, MNRAS, 357, 903
Chabrier, G. 2003, PASP, 115, 763
Cisternas, M., et al. 2011, ApJ, 726, 57
Civano, F., et al. 2012, ApJS, 201, 30
Civano, F., et al. 2010, ApJ, 717, 209
Comerford, J. M., Griffith, R. L., Gerke, B. F., Cooper, M. C., Newman, J. A., Davis, M., & Stern, D. 2009, ApJ, 702, L82
Conselice, C. J. 2003, ApJS, 147, 1
—. 2006, ApJ, 638, 686
Conselice, C. J., Bershady, M. A., Dickinson, M., & Papovich, C. 2003, AJ, 126, 1183
Conselice, C. J., Yang, C., & Bluck, A. F. L. 2009, MNRAS, 394, 1956
Cui, J., Xia, X.-Y., Deng, Z.-G., Mao, S., & Zou, Z.-L. 2001, AJ, 122, 63
Dale, D. A. & Helou, G. 2002, ApJ, 576, 159
Darg, D. W., et al. 2010a, MNRAS, 401, 1552
Darg, D. W., et al. 2010b, MNRAS, 401, 1043
De Propris, R., Conselice, C. J., Liske, J., Driver, S. P., Patton, D. R., Graham, A. W., & Allen, P. D. 2007, ApJ, 666, 212
de Ravel, L., et al. 2011, ArXiv e-prints
de Ravel, L., et al. 2009, A&A, 498, 379
Dey, A., et al. 2008, ApJ, 677, 943
Di Matteo, P., Combes, F., Melchior, A.-L., & Semelin, B. 2007, A&A, 468, 61
Di Matteo, T., Colberg, J., Springel, V., Hernquist, L., & Sijacki, D. 2008, ApJ, 676, 33
Di Matteo, T., Springel, V., & Hernquist, L. 2005, Nature, 433, 604
Donley, J. L., et al. 2012, ApJ, 748, 142
Elbaz, D., et al. 2010, A&A, 518, L29
Ellison, S. L., Mendel, J. T., Patton, D. R., & Scudder, J. M. 2013, ArXiv e-prints
Ellison, S. L., Patton, D. R., Mendel, J. T., & Scudder, J. M. 2011, MNRAS, 418, 2043
Ellison, S. L., Patton, D. R., Simard, L., & McConnachie, A. W. 2008, AJ, 135, 1877
Elvis, M., et al. 2009, ApJS, 184, 158
Fakhouri, O., Ma, C.-P., & Boylan-Kolchin, M. 2010, MNRAS, 406, 2267
Fiore, F., et al. 2008, ApJ, 672, 94
Genzel, R., et al. 2011, ApJ, 733, 101
Grogin, N. A., et al. 2011, ApJS, 197, 35
Guo, Q. & White, S. D. M. 2008, MNRAS, 384, 2
Hernquist, L. 1989, Nature, 340, 687
Hopkins, P. F. & Hernquist, L. 2006, ApJS, 166, 1
Hopkins, P. F., Hernquist, L., Cox, T. J., Di Matteo, T., Robertson, B., & Springel, V. 2006, ApJS, 163, 1
Hopkins, P. F., Hernquist, L., Cox, T. J., & Kereš, D. 2008, ApJS, 175, 356
Hopkins, P. F., Kocevski, D. D., & Bundy, K. 2013, ArXiv e-prints
Hopkins, P. F., et al. 2009, MNRAS, 397, 802
Hung, C.-L., et al. 2013, ApJ, 778, 129
Ilbert, O., et al. 2009, ApJ, 690, 1236
Ilbert, O., et al. 2013, ArXiv e-prints
Ilbert, O., et al. 2010, ApJ, 709, 644
Jahnke, K., et al. 2009, ApJ, 706, L215
Jogee, S., et al. 2009, ApJ, 697, 1971
Johansson, P. H., Burkert, A., & Naab, T. 2009, ApJ, 707, L184
Kampczyk, P., et al. 2007, ApJS, 172, 329
Kampczyk, P., et al. 2013, ApJ, 762, 43
Kartaltepe, J. S., et al. 2012, ApJ, 757, 23
Kartaltepe, J. S., et al. 2014, ArXiv e-prints
Kartaltepe, J. S., et al. 2010, ApJ, 721, 98
Kartaltepe, J. S., et al. 2007, ApJS, 172, 320
Kauffmann, G., White, S. D. M., Heckman, T. M., Ménard, B., Brinchmann, J., Charlot, S., Tremonti, C., & Brinkmann, J. 2004, MNRAS, 353, 713
Keel, W. C., Kennicutt, Jr., R. C., Hummel, E., & van der Hulst, J. M. 1985, AJ, 90, 708

Kennicutt, Jr., R. C. 1998, ApJ, 498, 541
Kennicutt, Jr., R. C. & Keel, W. C. 1984, ApJ, 279, L5
Kitzbichler, M. G. & White, S. D. M. 2008, MNRAS, 391, 1489
Kocevski, D. D., et al. 2012, ApJ, 744, 148
Koekemoer, A. M., et al. 2007, ApJS, 172, 196
Koekemoer, A. M., et al. 2011, ApJS, 197, 36
Koss, M., Mushotzky, R., Treister, E., Veilleux, S., Vasudevan, R., & Trippe, M. 2012, ApJ, 746, L22
Koss, M., Mushotzky, R., Veilleux, S., Winter, L. M., Baumgartner, W., Tueller, J., Gehrels, N., & Valencic, L. 2011, ApJ, 739, 57
Kuchinski, L. E., et al. 2000, ApJS, 131, 441
Lacey, C. & Cole, S. 1993, MNRAS, 262, 627
Lambas, D. G., Tissera, P. B., Alonso, M. S., & Coldwell, G. 2003, MNRAS, 346, 1189
Le Fèvre, O., et al. 2000, MNRAS, 311, 565
Le Floc'h, E., et al. 2009, ApJ, 703, 222
Le Floc'h, E., et al. 2005, ApJ, 632, 169
Leauthaud, A., et al. 2007, ApJS, 172, 219
Li, C., Kauffmann, G., Heckman, T. M., White, S. D. M., & Jing, Y. P. 2008, MNRAS, 385, 1915
Lilly, S. J., et al. 2009, ApJS, 184, 218
Lilly, S. J., et al. 2007, ApJS, 172, 70
Lin, L., et al. 2010, ApJ, 718, 1158
Lin, L., et al. 2004, ApJ, 617, L9
Lin, L., et al. 2008, ApJ, 681, 232
Liu, X., Greene, J. E., Shen, Y., & Strauss, M. A. 2010, ApJ, 715, L30
Liu, X., Shen, Y., & Strauss, M. A. 2012, ApJ, 745, 94
López-Sanjuan, C., Balcells, M., Pérez-González, P. G., Barro, G., García-Dabó, C. E., Gallego, J., & Zamorano, J. 2009, A&A, 501, 505
López-Sanjuan, C., et al. 2011, A&A, 530, A20
López-Sanjuan, C., et al. 2012, A&A, 548, A7
López-Sanjuan, C., et al. 2013, A&A, 553, A78
Lotz, J. M., et al. 2008a, ApJ, 672, 177
Lotz, J. M., Jonsson, P., Cox, T. J., Croton, D., Primack, J. R., Somerville, R. S., & Stewart, K. 2011, ApJ, 742, 103
Lotz, J. M., Jonsson, P., Cox, T. J., & Primack, J. R. 2008b, MNRAS, 391, 1137
—. 2010a, MNRAS, 404, 590
—. 2010b, MNRAS, 404, 575
Lotz, J. M., Primack, J., & Madau, P. 2004, AJ, 128, 163
Maier, C., et al. 2009, ApJ, 694, 1099
Masjedi, M., Hogg, D. W., & Blanton, M. R. 2008, ApJ, 679, 260
Massey, R., Stoughton, C., Leauthaud, A., Rhodes, J., Koekemoer, A., Ellis, R., & Shaghoulian, E. 2010, MNRAS, 401, 371
McCracken, H. J., et al. 2012, A&A, 544, A156
Mihos, J. C. & Hernquist, L. 1996, ApJ, 464, 641
Mihos, J. C., Richstone, D. O., & Bothun, G. D. 1992, ApJ, 400, 153
Moore, B., Katz, N., & Lake, G. 1996, ApJ, 457, 455
Moustakas, J., Kennicutt, Jr., R. C., & Tremonti, C. A. 2006, ApJ, 642, 775
Newman, A. B., Ellis, R. S., Bundy, K., & Treu, T. 2012, ApJ, 746, 162
Oke, J. B. 1974, ApJS, 27, 21
Papovich, C., Giavalisco, M., Dickinson, M., Conselice, C. J., & Ferguson, H. C. 2003, ApJ, 598, 827
Patton, D. R. & Atfield, J. E. 2008, ApJ, 685, 235
Patton, D. R., Carlberg, R. G., Marzke, R. O., Pritchet, C. J., da Costa, L. N., & Pellegrini, P. S. 2000, ApJ, 536, 153
Patton, D. R., et al. 2002, ApJ, 565, 208
Patton, D. R., Torrey, P., Ellison, S. L., Mendel, J. T., & Scudder, J. M. 2013, MNRAS, 433, L59
Pozzetti, L., et al. 2010, A&A, 523, A13
Robaina, A. R., et al. 2009, ApJ, 704, 324
Robaina, A. R., Bell, E. F., van der Wel, A., Somerville, R. S., Skelton, R. E., McIntosh, D. H., Meisenheimer, K., & Wolf, C. 2010, ApJ, 719, 844
Salvato, M., et al. 2009, ApJ, 690, 1250
Salvato, M., et al. 2011, ApJ, 742, 61
Sanders, D. B. & Mirabel, I. F. 1996, ARA&A, 34, 749
Sanders, D. B., et al. 2007, ApJS, 172, 86
Sanders, D. B., Soifer, B. T., Elias, J. H., Madore, B. F., Matthews, K., Neugebauer, G., & Scoville, N. Z. 1988, ApJ, 325, 74
Sargent, M. T., Béthermin, M., Daddi, E., & Elbaz, D. 2012, ApJ, 747, L31
Satyapal, S., Ellison, S. L., McAlpine, W., Hickox, R. C., Patton, D. R., & Mendel, J. T. 2014, ArXiv e-prints
Scarlata, C., et al. 2007, ApJS, 172, 406
Schramm, M. & Silverman, J. D. 2013, ApJ, 767, 13
Scoville, N., et al. 2007, ApJS, 172, 1
Scudder, J. M., Ellison, S. L., Torrey, P., Patton, D. R., & Mendel, J. T. 2012, MNRAS, 426, 549
Secker, J. 1995, PASP, 107, 496
Shi, Y., Rieke, G., Lotz, J., & Perez-Gonzalez, P. G. 2009, ApJ, 697, 1764
Silverman, J. D., et al. 2011, ApJ, 743, 2
Smolčić, V., et al. 2008, ApJS, 177, 14
Somerville, R. S., Hopkins, P. F., Cox, T. J., Robertson, B. E., & Hernquist, L. 2008, MNRAS, 391, 481
Springel, V., et al. 2005, Nature, 435, 629
Tasca, L. A. M., et al. 2014, A&A, 565, A10
Toomre, A. & Toomre, J. 1972, ApJ, 178, 623
Williams, R. J., Quadri, R. F., & Franx, M. 2011, ApJ, 738, L25
Woods, D. F. & Geller, M. J. 2007, AJ, 134, 527
Wu, H., Zou, Z. L., Xia, X. Y., & Deng, Z. G. 1998, A&AS, 132, 181
Xu, C. K., et al. 2012, ApJ, 760, 72
Zepf, S. E. & Koo, D. C. 1989, ApJ, 337, 34